

# **Green Synthesis of Iron Oxide Nanoparticles for Rhodamine 6G Dye Degradation and its Implications**

A Dissertation for

BOT-651 Discipline Specific Dissertation

Credits: 16

Submitted in partial fulfilment of Master's Degree

M.Sc. in Botany

By

**MAHESHWARI PRAKASH NAIK**

22P0480013

ABC ID: 927-356-704-311

PRN no. 201911467

Under the Supervision of

**DR. ADITI VENKATESH NAIK**

School of Biological Sciences and Biotechnology

Botany Discipline



**GOA UNIVERSITY**

April, 2024



Examined by:

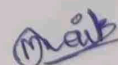
Seal of the School

*[Handwritten signatures]*

## **DECLARATION BY STUDENT**

I hereby declare that the data presented in this dissertation report entitled, "**Green Synthesis of Iron oxide Nanoparticles for Rhodamine 6G Dye Degradation and its Implications**" is based on the results of investigations carried out by me in the Botany discipline at the School of Biological Sciences and Biotechnology, Goa University under the supervision of Dr. Aditi Venkatesh Naik and the same has not been submitted elsewhere for the award of a degree or diploma by me. Further, I understand that Goa University or its authorities will be not be responsible for the correctness of observations/ experimental or other findings given the dissertation.

I hereby authorize the University authorities to upload this dissertation on the dissertation repository or anywhere else as the UGC regulations demand and make it available to any one as needed.



**Maheshwari Prakash Naik**

Seat no. 22P0480013

Botany Discipline

School of Biological Sciences and Biotechnology

Date: 08-04-2024

Place: Goa University

## COMPLETION CERTIFICATE

This is to certify that the dissertation report "**Green Synthesis of Iron oxide Nanoparticles for Rhodamine 6G Dye Degradation and its Implications**" is a bonafide work carried out by **Ms Maheshwari Prakash Naik** under my supervision in partial fulfilment of the requirements for the award of the degree of Masters of Science in Botany at the School of Biological Sciences and Biotechnology, Goa University.

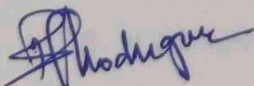


**Dr. Aditi Venkatesh Naik**

Botany Discipline

School of Biological Sciences and Biotechnology

Date: 08.04.2024



**Prof. B.F. Rodrigues**

Dean of the School

Botany Discipline

School of Biological Sciences and Biotechnology

Date: 8-4-2024

Place: Goa University



School Stamp

## **PREFACE**

I am pleased to present my dissertation on "*Green Synthesis of Iron Oxide Nanoparticles for Rhodamine 6G Dye Degradation and its Implications.*" This work represents the culmination of my efforts during my postgraduate degree in Botany, focusing on the application of nanotechnology in environmental remediation.

From December 2023 to March 2024, I dedicated myself to researching and writing this dissertation, overcoming challenges and expanding my knowledge of instruments such as XRD and FTIR, as well as refining my skills in data analysis programs.

Through the process of synthesizing iron oxide nanoparticles and studying their efficacy in degrading Rhodamine 6G dye, I gained insights that will undoubtedly shape my future endeavours. Throughout this journey, I have encountered obstacles that have taught me valuable lessons about perseverance and resilience, both professionally and personally.

I extend my gratitude to all who have supported me on this endeavour, and I hope this dissertation serves as a contribution to the field and an inspiration for future research in sustainable nanomaterials and environmental science.

I seize this opportunity to express my gratitude to everyone involved in this dissertation, whether through direct collaboration or in supportive capacities.

- ***Ms. Maheshwari Prakash Naik***



## **ACKNOWLEDGEMENT**

First, I would like to thank God for giving me strength, ability, and opportunity to carry out this study as well as for his blessings during my entire research process.

It is a great pleasure to express my deep and sincere gratitude to my mentor and guide Dr. Aditi Naik, Assistant Professor, Botany Discipline, SBSB, Goa University for her constant support, guidance and encouragement throughout the entire research process. Her guidance and advice helped me throughout my research and writing of the thesis.

I am also thankful to Senior Prof. B. F. Rodrigues, Dean, SBSB, Goa University and Senior Prof. S. Krishnan, Vice Dean, Botany Discipline, SBSB, Goa University for providing facilities to carry out the research work in the school.

I thank all the teachers Prof. B. F. Rodrigues, Prof. S. Krishnan, Dr. Rupali Bhandari, Dr. Siddhi Jalmi, Dr. Tanvi Prabhu, Mr. Allan Almeida, Botany Discipline, SBSB, Goa University, for their kind support, advice and suggestions during my dissertation work.

I am thankful to Ms. Jyothi Yarram, Technical assistant from Central Sophisticated Instrumentation Facility (CSIF) BITS Pilani KK Birla for her help and support during my research work. I also appreciate the kindness of the technical assistant staff at BITS Pilani.

I would like to express my gratitude to Dr. Rahul Kerkar, Asst Prof., P.E.S's R.S.N College of Arts & Science, Farmagudi for helping and providing valuable suggestions.

In addition, I would like to thank the entire non-teaching staff for their technical assistance, co-operation and help during my work.

I am deeply grateful to my parents and sister for their constant love, support and encouragement throughout my academic journey.

I would like to offer my special thanks to my friends and dear ones for their constant and endless help, motivation and support.

Finally I would like to acknowledge all the people who have supported me to complete the research work directly or indirectly.

**Miss Maheshwari Prakash Naik**

## **LIST OF TABLES**

<b>Table No.</b>	<b>Description</b>	<b>Page No.</b>
Table 4.1	Effect of degraded dye on the shoot, root length and biomass (shoot and root) in 15 days old rice seedlings.	41
Table 4.2	Effect of different concentration of degraded dye on the chlorophyll content of rice seedlings.	44
Table 4.3	Effect of different concentration of degraded dye on Malondialdehyde level of rice seedlings.	46
Table 4.4	Effect of different concentration of degraded dye on proline in mol g <sup>-1</sup> fr. Wt. of rice seedlings.	48

## **LIST OF FIGURES**

<b>Figure No.</b>	<b>Description</b>	<b>Page No.</b>
Figure 4.1	SEM images of biosynthesized iron oxide nanoparticles at a magnification of 15000 X (A) and 50.00 KX (B); C) EDS spectrum of iron oxide NPs.	29
Figure 4.2	FTIR spectra of the <i>Getonia floribunda</i> leaf extract and synthesized iron oxide (Fe <sub>2</sub> O <sub>3</sub> ) nanoparticles.	30
Figure 4.3	XRD patterns of iron oxide nanoparticles.	31
Figure 4.4	Graphical representation showing degradation efficiency of Rhodamine 6G dye.	34
Figure 4.5	Effect of different concentration of iron oxide nanoparticles in degradation of Rhodamine 6G.	35
Figure 4.6	Effect of time in degradation of Rhodamine 6G with different concentration of NPs.	36
Figure 4.7	Effect of degraded dye on the shoot and root length of rice.	42
Figure 4.8	Effect of degraded dye on the shoot and root biomass of rice.	42
Figure 4.9	Effect of different concentration of degraded dye on the chlorophyll content of rice seedlings.	44
Figure 4.10	Effect of different concentration of degraded dye on the lipid peroxidation (MDA) of rice seedlings.	46
Figure 4.11	Accumulation of proline in the leaves of rice seedlings treated with different concentration of degraded dye.	48

## **LIST OF PLATES**

<b>Plate No.</b>	<b>Description</b>	<b>Page No.</b>
Plate 4.1	Parts of the <i>Getonia floribunda</i> A) Habit B) Leaf C) Flowers D) Fruit	25
Plate 4.2	Green synthesis of iron oxide nanoparticles A) Plant extract B) Ferric chloride C) Synthesized iron oxide nanoparticles D) Dried powder of NPs.	26
Plate 4.3	Photocatalytic degradation of Rhodamine 6G dye treated with different concentration of NPs.	33
Plate 4.4	Photographic image of 15 days old <i>Oryza sativa</i> cv. Jaya seedlings treated with different concentration of degraded dye. A) Experimental setup; B) Root/ shoot length.	40

## **LIST OF ABBREVIATION**

<b>Entity</b>	<b>Abbreviation</b>
Carbon	C
Chlorine	Cl
Energy Dispersive X-ray spectroscopy	EDS
Fourier Transform Infrared Spectroscopy	FTIR
Iron	Fe
Iron Oxide Nanoparticles	IONP, FeONP
Malondialdehyde	MDA
Nanoparticle	NP
Oxygen	O
Rhodamine 6G	Rh 6G
Scanning Electron Microscopy	SEM
Sodium Hypochlorite	NaHClO
X-ray Diffraction	XRD



## **ABSTRACT**

This study presents the eco-friendly synthesis of Iron Oxide Nanoparticles (IONPs) using an aqueous leaf extract of *G. floribunda* for the purpose of decolorizing Rhodamine 6G dye. The synthesized IONPs underwent thorough characterization via Scanning Electron Microscopy (SEM), Energy Dispersive X-ray Spectroscopy (EDS), Fourier Transform Infrared Spectroscopy (FTIR), and X-ray Diffraction (XRD).

The findings revealed that phenolic compounds within the leaf extract served as both reducing and capping agents, facilitating the synthesis of nanoparticles. SEM analysis confirmed the spherical morphology of the IONPs, with an average diameter of 84.6 nm. EDS analysis corroborated the presence of oxygen and elemental iron, indicating predominantly oxide form of nanoparticles.

Remarkably, the synthesized IONPs exhibited excellent photocatalytic activity against Rhodamine 6G dye. At a concentration of 1.0 g/L of nanoparticles, a remarkable degradation efficiency of 72.4% was achieved. Subsequently, various concentrations of the degraded dye were applied to rice seedlings to assess their impact on morphological and physiological parameters.

Results indicated a positive correlation between degraded dye concentration and growth and chlorophyll content, while Proline and Malondialdehyde (MDA) content decreased. Thus, the synthesized nanoparticles demonstrate promising efficacy as sorbents for decolorizing Rhodamine 6G dye from aqueous solutions.

## **CHAPTER 1: INTRODUCTION**

### **1.1 General Overview**

Nanotechnology is the science that deals with matter at the scale of 1 billionth of a meter (i.e.,  $10^{-9}\text{m} = 1\text{ nm}$ ). A nanoparticle is the most fundamental component in the fabrication of a nanostructure. Nanoscience and nanotechnology have the ability to fabricate, characterize, and manipulate artificial structures, the features of which are controlled at the nanometre level. Nanoparticles are composed of carbon, metal, metal oxides, or organic materials which range in size from 1 to 100 nm (Priya *et al.*, 2021).

Nanoparticles (NPs) are wide class of materials that include particulate substances, which have one dimensions less than 100 nm (Laurent *et al.*, 2010). Nanostructure materials are classified as 0D, 1D, 2D or 3D (Tiwari *et al.*, 2012). In 0D, the length, breadth, and height of nanoparticle is fixed at a single point for example nano dots whereas 1D possess only one parameter for example graphene, 2D where it has length and breadth for example carbon nanotubes, or 3D where it has all parameters such as length, breadth and height for example gold nanoparticles. Because of their small size nanoparticles show enhanced properties such as high reactivity, strength, surface area, sensitivity, stability, etc.

#### **1.1.1 Approaches for the synthesis of nanoparticles**

Physical, chemical and biological are the three main approaches for the synthesis of NPs. The physical approach is also called as the top-down approach whereas the chemical and biological approach are collectively called as the bottom-up approach (Salem & Fouda, 2020).

### **1.1.1.a Bottom-up method**

In this approach tiny atoms and molecules are combined in bottom-up methods to create nanomaterials, and biological synthesis are some of the most widely used methods of nanoparticle synthesis. The bottom-up technique allows for better accuracy in the nanometric state, allowing for a variety of nanoparticle shapes, greater precision in molecule placement, uniformity in grain size, and product homogeneity, although at the expense of reduced production volumes.

### **1.1.1.b Top-down method**

In this approach the bulk materials are fragmented in top-down methods to create nano-structured materials. The top-down strategy allows for higher numbers of production, but the final nanoparticle product may lack homogeneity in size and shape due to the production methodology involving mechanical stress, severe shocks, and deformation. It includes methods such as mechanical milling, nanolithography, laser ablation, sputtering, thermal decomposition.

## **1.1.2 Classification of Nanoparticles**

Based on composition, nanoparticles are classified as organic, inorganic and carbon based (Ealia & Saravanakumar, 2017).

### **1.1.2.a Organic nanoparticles**

This class encompasses nanoparticles composed of proteins, carbohydrates, lipids, polymers, or other organic compounds. Examples include dendrimers, micelles, liposomes, and ferritin. These nanoparticles are characterized by their non-toxicity, biodegradability,

and, in some cases, a hollow core. Organic nanoparticles find extensive application in the biomedical field, particularly in drug delivery and cancer therapy.

#### **1.1.2.b Inorganic nanoparticles**

These nanoparticles are not made up of carbon. Metal and metal oxides are the typical examples of this class which include Aluminium (Al), Cadmium (Cd), Cobalt (Co), Copper (Cu), Gold (Au), Iron (Fe), Silver (Ag), Zinc (Zn), Iron oxide ( $\text{Fe}_2\text{O}_3$ ), Magnetite ( $\text{Fe}_3\text{O}_4$ ), Titanium oxide ( $\text{TiO}_2$ ), Zinc oxide ( $\text{ZnO}$ ).

#### **1.1.2.c Carbon based nanoparticles**

This class of nanoparticles are completely made from carbon atoms. Fullerenes, carbon black NPs, and quantum dots are some of the examples of this class.

### **1.1.3 Methods of nanoparticle generation**

IONPs can be synthesized by three methods such as physical, chemical and biological (Gaur & Jain, 2019).

#### **1.1.3.a Physical method**

The physical approach is more advantageous than chemical approach because of the absence of solvent contamination and the uniformity of the synthesized nanoparticles. In this method of synthesis, the size of the particles cannot be controlled in nanometre range (Agarwal *et al.*, 2017).

#### **1.1.3.b Chemical method**

A large number of nanoparticles, can be synthesized by this method; but because of the use of reagents this method of synthesis is toxic and harmful for the environment (Arularasu *et al.*, 2018). These methods are simple and efficient in which the size, shape,

and composition of the NPs can be managed. Coprecipitation is the most widely used method for the synthesis of NPs.

#### **1.1.3.c Biological method**

Biological or green synthesis is the bottom-up method for the synthesis of nanoparticles. Plants, algae, bacteria, fungi are used as biological agents for the synthesis of nanoparticles (Pandit *et al.*, 2022; Roy *et al.*, 2021). Different parts of the plants including leaf, root, stem, flowers, fruit, seeds, rhizomes have been extensively used in the green synthesis of nanoparticles due to the presence of various biomolecules (Sidhu *et al.*, 2022). The phytochemicals present in the plant extracts act as stabilizing and capping agents for the synthesis of NPs hence there is no need to add capping and stabilizing agents from the outside. The bioactive compounds present in plants such as alkaloids, flavonoids, terpenoids, steroids, etc act as reducing agents for the synthesis of nanoparticles. Since biological method is non toxic and cost effective it is considered as the best method for the synthesis of nanoparticles.

#### **1.1.4 Capping agents**

Capping agents play a vital role in the synthesis of NPs. These are defined as “binding molecules” that are used in minute quantity for the synthesis of nanoparticles (Sharma *et al.*, 2021). Majority of the chemical methods use chemical capping agents for the synthesis of NPs. These molecules show a strong interaction with the surface of metal nanoparticles and thus serve as good stabilizing agents but these chemical agents are tough to detach from the surface of the nanoparticles and are non-biodegradable and toxic to the biological systems. Whereas green synthesis method makes use of biomolecules as capping agents for the synthesis of NPs which are non toxic to the biological system and the environment.



### 1.1.5 Iron oxide nanoparticles

Iron oxide nanoparticles are the types of inorganic based nanoparticles. These nanoparticles consist of maghemite ( $\gamma\text{-Fe}_2\text{O}_3$ ) and/or magnetite ( $\text{Fe}_3\text{O}_4$ ) particles with diameters ranging between 1 and 100 nm (Kumar & Prem, 2018). These nanoparticles are of great importance because of their super-paramagnetic properties and potential biomedical applications. Due to the unique electrical, optical, and magnetic property of IONPs they are widely used in biology, medicine, diagnostics, and drug delivery system. Also, they are being used in environmental remediation, food and agriculture, textiles and electronics and wastewater treatment as adsorbents (Suppiah *et al.*, 2023). As IONPs exhibit sorbent properties they are successfully tested for removal of organic dyes and toxic inorganic metal pollutants from industrial waste water (Beheshtkhoo *et al.*, 2018).

### 1.1.6 Applications of nanoparticles

Nanoparticles, owing to their distinct and tailored properties, find application across diverse fields. In the medical sector, they are utilized for diagnostics, drug delivery systems, and antimicrobial purposes (Yaqoob *et al.*, 2020). In the chemical industry, nanoparticles serve as catalysts. Additionally, they play a crucial role in environmental protection initiatives.

#### 1.1.6.a Medicine and drug delivery

NPs have captured the interest of every discipline of medicine due to their ability to deliver medications in the optimal dosage range, which often results in better therapeutic efficiency, reduced side effects, and improved patient compliance (Alexis *et al.*, 2008). Superparamagnetic iron oxide nanoparticles with proper surface chemistry can be employed for a variety of *in vivo* applications including MRI contrast enhancement, tissue healing,

immunoassay, detoxification of biological fluids, hyperthermia, drug delivery, and cell separation. All of these biomedical applications require high magnetization value, particle size less than 100 nm, and a narrow particle size distribution (Laurent *et al.*, 2010). Magnetite ( $\text{Fe}_3\text{O}_4$ ) or its oxidised form Maghemite ( $\text{Fe}_2\text{O}_3$ ) are the most frequently employed iron oxide particles in biomedical applications (Ali *et al.*, 2016).

#### **1.1.6.b Environment**

Surface water is treated with nanoparticles through disinfection, filtration, and desalination. Heavy metals, viruses, and organic pollutants are among the most likely contaminants. Because of the adverse effects on the environment and human health, heavy metals such as Mercury, Lead, Thallium, Cadmium, and Arsenic have been removed from natural water. Superparamagnetic iron oxide NPs are an efficient sorbent for this toxic material. Photodegradation by nanoparticles is also a common practice, and several nanomaterials are used for this purpose. Badmapriya & Asharani, (2016) utilized iron oxide as green catalyst for the effective degradation of Malachite Green and Methyl Orange.  $\text{TiO}_2$  and ZnO nanoparticles and nanocomposites are used for degradation of organic pollutants in water and air (Subhan *et al.*, 2021).

#### **1.1.6.c Food**

Improvement in the production, processing and packaging of food is achieved by incorporating nanotechnology. Nanoparticles and nanocomposites have antibacterial properties that can be used for improving food safety e.g., Ag NPs and nanocomposites. Silver nanoparticles have high antimicrobial activity and are commonly used as an active system in food packaging. They are also used in consumer product as preservative agents. Nanoparticles such as Zinc oxide, Titanium oxide, and Silicate nanoparticles are also being used in plastic films to reduce the flow of oxygen inside the packaging container. These

nanoparticles keep the food fresh for a longer time and also help to prevent the leakage of moisture from the packaging (Dash *et al.*, 2022).

#### **1.1.6.d Construction**

Among the many different types of nanoparticles, Titanium dioxide, Carbon nanotubes, Silica, Copper, Clay, and Aluminium oxide are the most widely used nanoparticles in the construction sector. Nanoparticles can be used as binders in cement to enhance its properties, such as strength, durability, and workability (Papadaki *et al.*, 2018). Nanoparticles such as nano silica, nano clays, nano Titanium Oxide ( $\text{TiO}_2$ ), nano Iron ( $\text{Fe}_2\text{O}_3$ ), nano Alumina ( $\text{Al}_2\text{O}_3$ ), Copper Oxide ( $\text{CuO}$ ), Zinc peroxide ( $\text{ZnO}_2$ ) and ( $\text{ZrO}_2$ ) Zirconium dioxide are considered as candidates for the improvement of concrete properties (Khayati *et al.*, 2015). Nanotechnology improves the durability, strength, life span and resistance of construction materials by providing desired properties.

#### **1.1.6.e Fabrics**

In textile industries to enhance textile features nanoparticle plays an important role. These features are fabric softness, durability, breathability, water repellence property, fire retardant, and anti-microbial properties. Nanoparticles such as silica exhibit water-repellent properties. They are either sprayed on the fabric surface or woven into it to ensure water does not enter the fabric. It is widely used in umbrellas and raincoats.

### 1.1.7 *Getonia floribunda*

Kingdom : Plantae

Clade : Tracheophytes

Clade : Angiosperms

Clade : Eudicots

Clade : Rosids

Order : Myrtales

Family : Combretaceae

Genus : *Getonia*

Species : *floribunda*

*Getonia floribunda* commonly known as “Ukshi” belongs to the family Combretaceae. It is native to Bangladesh and India. It is widely distributed in the central and southern parts of India and also found in south-east Asian countries (Azhagumeena & Bharathi, 2020).

#### 1.1.7.a Botanical Description

*Getonia floribunda* Roxb. is a climbing shrub that grows to a height of 5-10 m. It has slender, rust-colored striped branches with thick fluff on the surface. The vine-covered branches are known to store plenty of water. Keratinous leaves are 5-12 cm long, ovoid or oval in shape, opposite, acuminate, and spherical. The dense flower cluster appears at the tips of branches (Yarazari & Jayaraj, 2022). Flowers are devoid of petals. Fruit inception bears 1 ventricle and 3 pendulous ovules inside. Fruit is about 8 mm long and the sepals are prominently hairy and green (Azhagumeena & Bharathi, 2020).

### 1.1.7.b Medicinal use

The medicinal applications of *Getonia floribunda* encompass a wide range of ailments, including jaundice, ulcers, colic, leprosy, malarial fever, dysentery, vomiting, and skin diseases (Glory *et al.*, 2016). Additionally, it is utilized as an anthelmintic, astringent, and laxative, addressing various gastrointestinal issues. The plant is also known for its hepatotoxicity, neurotoxicity, and cardiotoxicity properties. Furthermore, it exhibits antimicrobial, antioxidant, antiviral, and anti-inflammatory properties, making it a versatile remedy in traditional medicine (Dey *et al.*, 2005). Alkaloids, flavonoids, tannins, and phenolic compounds stand out as the primary secondary metabolites of *Getonia floribunda*, contributing significantly to its medicinal properties. These compounds serve as key components in the preparation of numerous herbal medicines derived from the plant. Of particular note is the presence of the anti-inflammatory flavonoid compound calycopterin, predominantly found in the leaves of *Getonia floribunda*. This compound has garnered attention for its therapeutic potential, further enhancing the plant's medicinal value.

The extensive medicinal repertoire of *Getonia floribunda* serves as a compelling backdrop for exploring its applications in the synthesis of iron oxide nanoparticles. By harnessing the plant's bioactive constituents, such nanoparticles could potentially offer novel solutions for environmental remediation, such as the degradation of hazardous dyes like Rhodamine 6G. This study seeks to bridge the traditional wisdom of herbal medicine with modern nanotechnology, paving the way for innovative approaches to sustainability and healthcare.



## 1.2 Aim and Objectives

Untreated effluents from the textile industry containing colorant dyes are detrimental to the environment, aquatic organisms and human health. Among these effluents Rhodamine 6G is known as corrosive and irritant dye (Abdullah *et al.*, 2021). Rhodamine 6G is an azo dye with one or more  $-N=N-$  groups affixed to an aromatic structure (Silva *et al.*, 2019). Because of its chromophoric properties, the dye has both chemical stability and recalcitrance. It is a derivative of Xanthene dye, which is widely utilized in the paper, textile, and printing industries as well as in fluorescent labelling. In order to achieve the desired aim of the study, the following objectives were formulated.

### **Objective 1: Green Synthesis of Iron Oxide Nanoparticles using *Getonia floribunda* Roxb.**

- Extract iron oxide nanoparticles via a green synthesis approach utilizing *Getonia floribunda* and characterize them using XRD, FTIR, and SEM analysis.

### **Objective 2: Evaluation of Iron Oxide Nanoparticles for Rhodamine 6G Dye Degradation.**

- Assess the effectiveness of the synthesized nanoparticles in degrading Rhodamine 6G dye.

### **Objective 3: To study the effect of biologically degraded Rhodamine 6G on Selected Plants.**

- Investigate the influence of degraded Rhodamine 6G on growth and physiological parameters of rice seedlings.

### 1.3 Hypotheses

The synthesis of iron oxide nanoparticles using *Getonia floribunda* is anticipated to yield eco-friendly and cost-effective nanoparticle production method further evaluation of these nanoparticles for Rhodamine 6G dye degradation is expected to demonstrate high efficiency. Furthermore, the effect of degraded dye on rice seedlings aims to highlight contrasting impacts on plant physiology and growth, facilitating better understanding for environmental implications.

### 1.4 Scope

Expanding upon the outlined scope, the study aims to address the pressing environmental concerns posed by untreated dyes in various industries. By focusing on the green synthesis of iron oxide nanoparticles as a photocatalyst for the decolorization of Rhodamine 6G dye, the research endeavours to offer a sustainable solution to mitigate dye pollution. Moreover, the study seeks to compare the efficacy and environmental impact of green synthesis methods with conventional approaches that often rely on hazardous chemicals. Additionally, the scope extends to exploring the broader implications of utilizing biocompatible catalysts in environmental remediation efforts. Through comprehensive analysis and experimentation, the study aims to contribute to the growing body of knowledge on green chemistry and sustainable technologies, ultimately fostering a safer and healthier environment for both humans and ecosystems.

## **CHAPTER 2: LITERATURE REVIEW**

### **2.1 Phytochemical and bioactivity studies of *Getonia floribunda*:**

Azhagumeena *et al.*, (2020) revealed that *Calycopteris floribunda* possesses a multitude of flavone and phenolic molecules, indicating high antioxidant potential, underscoring its therapeutic promise with minimal toxic effects.

Pavithra *et al.*, (2013) showcased the antioxidant and antibacterial efficacy of solvent extracts from *Calycopteris floribunda*, *Humboldtia brunonis*, and *Kydia calycina* flowers. Notably, the methanol extract of *C. floribunda* exhibited robust antibacterial activity, outperforming *H. brunonis* and *K. calycina*.

Yarazari & Jayaraj (2022) conducted a preliminary investigation into the phytochemical constituents and bioactive compounds of *Calycopteris floribunda* flower extracts through GC–MS analysis. The ethanol extract exhibited a higher number of bioactive compounds than the acetone extract, highlighting the presence of 41 compounds, including carbohydrates, hexose sugar, steroids, Coumarin's glycoside, alkaloids, phenols, flavonoids, tannin, organic acids, and triterpenoids. Similar compounds were also noted in leaf extracts by Glory *et al.*, (2016).

Bhat *et al.*, (2011) evaluated antimicrobial activities of *Calycopteris floribunda* leaf extracts using three different solvents against *Bacillus cereus*, *Bacillus subtilis*, and *Staphylococcus aureus*. The diethyl ether-methanol extract and its petroleum ether-butanol fraction exhibited significant antibacterial activity, with varying antioxidant properties among the solvents.

Glory *et al.*, (2016) investigated various solvent extracts (petroleum ether, chloroform, ethyl acetate, methanol, and aqueous) of *Calycopteris floribunda* leaves. Their findings

highlighted the presence of terpenoids, sterols, alkaloids, and flavonoids. Notably, the methanolic leaf extract displayed superior antibacterial activity against pathogenic bacteria strains compared to other solvent extracts.

Dey *et al.*, (2005) examined the dichloromethane-methanol extract of *Calycopteris floribunda* leaves and its aqueous 90% methanol soluble fractions. These fractions exhibited significant antibacterial activity against *Bacillus subtilis*, *Streptococcus pyogenes*, *Staphylococcus aureus*, and *Salmonella typhi*, along with notable  $\beta$ -glucuronidase inhibition and antioxidant activity.

Bharat *et al.*, (2019) biosynthesized silver nanoparticles from *Calycopteris floribunda* leaf extracts, showcasing promising antimicrobial and anticancer activity against neoplastic cell lines. Further investigation of the ethyl acetate extract led to the isolation and identification of the bioactive compound, Gallic acid, confirmed through TLC, column, and HPLC analysis.

## 2.2 Synthesis of nanoparticles

Hasan (2015) provided an overview of nanoparticles, focusing on their biosynthesis mechanisms and various types.

Jacinto *et al.*, (2020) discussed the primary biosynthesis protocols employed in synthesizing iron oxide nanoparticles (IONPs), emphasizing the successful utilization of plants and microorganisms in producing magnetic IONPs.

Vasantharaj *et al.*, (2018) synthesized FeONPs using *Ruellia tuberosa* green leaf extract, demonstrating potential antibacterial activity against both Gram-negative and Gram-positive pathogens. Moreover, the synthesized nanoparticles showed dye degradation

capability against crystal violet. FTIR analysis revealed distinct metal-oxygen peaks at 422, 506, and 622  $\text{cm}^{-1}$ , indicating the presence of FeONPs.

Goutam *et al.*, (2019) investigated the green synthesis approach for nanoparticles and explored their applications in water and wastewater treatment, specifically in dye degradation from wastewater sources.

Devatha *et al.*, (2016) synthesized iron nanoparticles utilizing various leaf extracts such as *Mangifera indica*, *Murraya Koenigii*, *Azadiracta indica*, and *Magnolia champaca*. They characterized these nanoparticles using UV-Visible spectrophotometry, SEM equipped with X-ray energy dispersive spectroscopy, and FTIR. The efficiency of the synthesized nanoparticles was evaluated for the concurrent removal of total phosphates, ammonia, nitrogen, and chemical oxygen demand from domestic wastewater. Among the different plant-mediated synthesized iron nanoparticles, *Azadiracta indica* exhibited substantial removal rates of 98.08% for phosphate, 84.32% for ammonia nitrogen, and 82.35% for chemical oxygen demand.

### **2.3 Nanoparticles in dye degradation**

Karpagavinayagam & Vedhi (2018) synthesized iron oxide NPs using the flower extract of *Avicennia marina*. SEM results indicated an average size of FeO-NPs ranging from 30 to 100 nm. These nanoparticles were utilized in various applications including industrial uses, dye degradation, and environmental pollution control.

Beheshtkhoo *et al.*, (2018) synthesized iron oxide NPs using *Daphne mezereum* aqueous leaf extract. The average diameter of the prepared NPs ranged from 6.5 to 14.9 nm with a mean particle size of 9.2 nm. Furthermore, the synthesized iron nanoparticles demonstrated an 81% decoloration efficiency for MO after 6 hours.



Kumar & Prem (2018) conducted green synthesis of iron oxide nanoparticles from *Phyllanthus niruri* leaf extract, comparing the results with a chemical method. Analytical studies revealed nearly identical size and morphology for the synthesized iron oxide nanoparticles from both methods. These nanoparticles exhibited significant antimicrobial activity against microbes like *Escherichia coli* and *Pseudomonas aeruginosa*. The authors concluded that the plant extract-based synthesis is more beneficial due to its cost-effectiveness, energy efficiency, and eco-friendliness compared to hazardous chemical synthesis.

Badmapriya & Asharani (2016) synthesized iron oxide nanoparticles using an aqueous extract of *Piper beetle* leaves. Phenolic compounds in the leaf extract acted as reducing and capping agents, facilitating nanoparticle formation. TEM analysis confirmed the spherical shape of the iron oxide nanoparticles, with average particle size of 16 nm. These nanoparticles were also utilized as a green catalyst for efficient decolorization of Malachite Green and Methyl Orange.

Adhikari *et al.*, (2022) explored the use of synthesized IONPs using *Psidium guajava* leaf extract for industrial dye degradation. These IONPs effectively degraded Methylene Blue (MB) and Methyl Orange (MO) in the presence of  $H_2O_2$ , achieving 82.1% degradation in 95 minutes for MB and 53.9% in 205 minutes for MO. Additionally, the synthesized IONPs exhibited good antibacterial activity against both *Shigella sonnei* and *Staphylococcus aureus* gram-positive bacteria, with a ZOI of 13 mm.

Priya *et al.*, (2021) highlighted that IONPs produced by plants, fungi, bacteria, and algae typically fall within the range of 1-100 nm, exhibiting various shapes like cubic, spherical, and cylindrical. These nanoparticles play crucial roles as reducing, capping, stabilizing, and fabricating agents in the green synthesis of nanoparticles.

Bibi *et al.*, (2019) synthesized iron oxide nanoparticles ( $\text{Fe}_2\text{O}_3$  NPs) using Pomegranate (*Punica granatum*) seeds extract. The synthesized nanoparticles were semi-spherical, ranging in size from 25 to 55 nm. These  $\text{Fe}_2\text{O}_3$  NPs displayed excellent photocatalytic activity against reactive blue under UV light irradiation, achieving a maximum degradation of 95.08% within 56 minutes of reaction time.

Singh *et al.*, (2018) summarized the fundamental processes and mechanisms of "green" synthesis approaches, particularly for metal and metal oxide nanoparticles (e.g., Gold (Au), Silver (Ag), Copper oxide (CuO), and Zinc oxide (ZnO) using natural extracts. They delved into the role of biological components and essential phytochemicals (e.g., flavonoids, alkaloids, terpenoids, amides, and aldehydes) as reducing agents and solvent systems.

Phoemphoonthanyakit *et al.*, (2019) utilized Iron oxide ( $\text{Fe}_3\text{O}_4$ ) magnetic nanoparticles in adsorbing Rhodamine 6G solution and evaluated their efficiency using UV-Vis spectrometry. The adsorption mechanism of Rhodamine 6G on  $\text{Fe}_3\text{O}_4$  was scrutinized concerning adsorbent dosage (2.5-10mg/L) and treatment time (0-150 min), showcasing the highest efficiency of dye removal at 10 mg/L  $\text{Fe}_3\text{O}_4$ , with an adsorption capacity of about 150 mg/g and a reduced treatment time of 30 min. They demonstrated the capacity of  $\text{Fe}_3\text{O}_4$  MNPs to eliminate toxic pollutants from wastewater by absorbing Rhodamine 6G.

Abdullah *et al.*, (2021) developed a coconut shell-derived nanomagnetic adsorbent composite (CS-NMAC) for removing Rhodamine 6G from aqueous solutions. Physical and adsorption properties of CS-NMAC were characterized via BET surface area analysis, X-ray diffraction, and FTIR, revealing a maximum adsorption capacity of 32.02 mg/g.

Kirubaharan *et al.*, (2020) synthesized Silver and Palladium nanoparticles using a *Daucus carota* leaves-mediated biosynthesis process. They characterized the morphology,

crystalline structure of the synthesized nanoparticles through UV-Vis spectrometry, TEM, XRD, and FT-IR analyses. The green-synthesized D-Ag and D-Pd nanoparticles facilitated the catalytic decolorization of Rh-6G dye and pathogen deactivation. Pd nanoparticles achieved nearly 98% Rh-6G dye decolorization within 2 minutes, while Ag nanoparticles took 30 minutes for 89.4% decolorization.

Silva *et al.*, (2019) employed *Clitoria fairchildiana* (CF) pods as a biosorbent to remove R6G from synthetic dye effluents. They characterized CF through various analyses and observed its maximum adsorption capacity ( $73.84 \text{ mg g}^{-1}$ ) at pH 6.4 and 298.15 K, concluding that CF is an efficient, green, and readily available biosorbent for wastewater dye removal.

Barzan & Hajiesmaeilbaigi (2016) synthesized Gold nanoparticles using the laser ablation method, characterizing them through Transmission Electron Microscopy and UV-visible absorption spectroscopy. Their measurements demonstrated that the presence of Gold nanoparticles decreased the fluorescence power and fluorescence quantum yield while increasing the absorbance and absorbed power of Rhodamine 6G.

Amrutham *et al.*, (2020) synthesized Palladium nanoparticles via the microwave irradiation method using Neem gum. The characterized PdNPs exhibited an average particle size of about 4 nm and displayed excellent catalytic activity towards the reduction of Rhodamine 6G.

Touchente *et al.*, (2019) investigated the impact of sonication on the photodegradation of Rhodamine 6G (Rh6G), a fluorone dye, using woven cotton fabrics adorned with TiO<sub>2</sub> nanoparticles (NPs). TiO<sub>2</sub> NPs were *in situ* synthesized via the sol-gel method in the presence of cotton textile and then subjected to hydrothermal treatment. Ultrasonic treatment

of TiO<sub>2</sub>-loaded fabrics was performed to assess NP adhesion and fabric properties. The fabrics exhibited high photocatalytic activity towards Rh6G, serving as a model dye.

Rasheed *et al.*, (2017) showcased the substantial efficiency of UV-based photocatalytic treatment for the decolorization and degradation of Rh-6G dyes in an aqueous medium. Photo-assisted treatment led to complete degradation of Rh-6G, along with 90.14% total organic carbon (TOC) removal within 180 minutes of contact time. Additionally, toxicity assays revealed a notable reduction in the toxicity of dye samples post-photocatalytic treatment.

Kansal *et al.*, (2007) conducted a comparative analysis of the photocatalytic activity of various semiconductors, highlighting ZnO as the most active photocatalyst for decolorizing MO and R6G. They observed that ZnO catalyst resulted in over 90% decolorization of dyes, especially at a basic pH. The maximum adsorption of MO occurred at pH 4, while for R6G, it was at pH 10. Interestingly, R6G displayed higher decolorization efficiency with a lower catalyst dose (0.5 g/L) compared to MO (1 g/L) under similar conditions. The ZnO/solar light photocatalytic system outperformed the ZnO/UV system.

Aigbe *et al.*, (2023) synthesized magnetic nanoparticles (MNPs) using *Vernonia amygdalina* leaf extract via the co-precipitation method and characterized them using TEM, XRD, FTIR, and UV-Vis spectrometry. They determined the optimum sorption capacity to be 454 mg.g<sup>-1</sup>. Furthermore, the R6G dye molecules were effectively desorbed from the spent sorbent using 0.1 M HCl for four adsorption-desorption cycles. The synthesized MNPs proved to be an effective sorbent for removing cationic dyes from aqueous solutions.

## **CHAPTER 3: METHODOLOGY**

### **3.1 Collection and preparation of plant extract**

The fresh leaves of *Getonia floribunda* Roxb. belonging to the family Combretaceae were collected from the Goa University Campus, Taleigao Plateau, Goa 403206. The collected leaves were washed several times with distilled water to remove dust and impurities. The leaves were dried in hot air oven at 40<sup>0</sup>c for 6-7 hours and after drying they were ground into fine powder with the help of mechanical grinder.

For the preparation of leaf extract 5 g of leaf powder was dissolved in 250 mL of distilled water which was kept on magnetic stirrer at 60<sup>0</sup> C for 30 minutes. The extract was filtered through whatman filter paper no. 1 and was stored in refrigerator at 4<sup>0</sup>C for further analysis (Bhuiyan *et al.*, 2020).

### **3.2 Synthesis of Iron oxide nanoparticles**

For the preparation of FeONPs, *Getonia floribunda* leaf extract was added dropwise to 0.1 M FeCl<sub>3</sub> solution in 1:1 (v/v) ratio at room temperature. The pH of the mixture was maintained at pH 9 by adding 1 M NaOH. The mixture was stirred using magnetic stirrer for 30 minutes at 60<sup>0</sup>C. The formation of black coloured solution confirmed the synthesis of FeONPs (Bhuiyan *et al.*, 2020).

### **3.3 Characterization of FeONPs**

#### **3.3.1 Fourier Transform Infrared Spectroscopy (FTIR) Analysis**

To determine the potential biomolecules in the plant extract responsible for the reduction and capping of the nanoparticles, FTIR spectroscopy measurements were carried out on the prepared nanoparticles. Using the KBr pellet approach, an FTIR spectrometer was used to record FTIR spectrum in the range of 4000-400 cm<sup>-1</sup>.

### **3.3.2 Scanning Electron Microscopy (SEM) and Energy Dispersive Spectroscopy (EDS)**

The morphology and size of the synthesized nanoparticles was determined by using Scanning Electron Microscopy (SEM). The copper stubs were used to mount the nanoparticles, and a SEM with a secondary electron detector was used to examine the images. Specific areas were located from SEM images and the elemental composition was carried out using EDS analysis.

### **3.3.3 X-Ray diffraction (XRD) analysis**

XRD was used to determine the crystal structures of iron oxide nanoparticles. XRD patterns were recorded by an X-ray diffractometer by using Cu  $k\alpha$  radiation from a broad focus Cu tube operated at 40 KV and 40 MA.

### **3.4 Photocatalytic effect of NPs in Rhodamine 6G dye degradation**

To study the photocatalytic activity of nanoparticles, 10 ppm concentration of Rhodamine 6G dye solution was prepared. Different concentrations of nanoparticles (0.2 g/L, 0.4 g/L, 0.6 g/L, 0.8 g/L, 1.0 g/L) were taken separately in a beaker containing 50 mL of the dye solution and were kept under sunlight along with continuous stirring. A control was set without nanoparticles which was kept under sunlight, similarly a second control was set which was maintained in the dark. After every 3 hours of time interval, 10 mL of the solution was withdrawn to evaluate the photocatalytic degradation of the dye. Before measuring the absorbance, the solution was centrifuged for 1 minute to remove the particles and the degradation efficiency was calculated by using the following formula:

$$\text{Degradation efficiency (\%)} = (C_0 - C_t) / C_0 * 100$$

Where  $C_0$  is the initial concentration and  $C_t$  is the concentration of the dye at time  $t$  (Bhuiyan *et al.*, 2020).

### **3.5 Effect of degraded dye on rice seedlings**

#### **3.5.1 Plant material**

The rice (*Oryza sativa* L. cv. Jaya) seedlings were used to see the effect of degraded dye. This is a short duration, dwarf and high yielding rice variety grown extensively in Goa. The seeds were obtained from Ela farm, Old Goa.

#### **3.5.2 Growth conditions and treatment**

*Oryza sativa* L. cv. Jaya seeds were thoroughly washed with water to remove floating and non-viable seeds. The viable seeds were surface sterilized with 4% sodium hypochlorite (NaHClO) for 5 minutes with constant stirring. Subsequently, they were immersed in distilled water and soaked for a period of four days. Soaked seeds were transferred in a 3-inch plastic pot containing 3:1 ratio of soil and vermicompost. The plants were raised in the growth room with a photoperiod of 16 hours, maintaining a temperature of  $28 \pm 2^\circ\text{C}$ . The relative humidity was carefully controlled and maintained at 70-75% throughout the growth period. Foliar treatment of different concentrations of nanoparticles mediated degraded dye was given and nutrient solution was provided in the form of Hoagland's solution (Kevat, 2018). The centrifuged degraded dye was sprayed on plants with the help of spray bottle. Spraying was done 3 to 5 times in alternate days. Also plants were treated with hoaglands solution once in a week.

#### **3.5.3 Measurement of Shoot and root length and biomass**

Plants were gently washed with water to remove soil that were attached to intact plants. Shoot and root measurements were physically taken for individual sets of plants. In order to

measure fresh biomass, ten individual plants from each concentration were split into roots and shoots, and the sample's weight was recorded (DaCosta, 2016).

#### **3.5.4 Extraction and estimation of Chlorophyll content**

100 mg of fresh leaf material was taken and ground with 4 mL of 80% acetone using mortar and pestle until the tissue was completely macerated. The homogenate was centrifuged at 5000 rpm for 5 minutes. The supernatant was transferred and the procedure was repeated till the residue became colourless. Using UV-Vis spectrophotometer the absorbance of the solution was read at 645 nm and 663 nm against the solvent (80% acetone) blank (Siva and Benita, 2016).

$$\text{Total chlorophyll (mg/g fr.wt.)} = [(20.2 \times A_{645} - 8.02 \times A_{663}) / 1000 \times W] \times V$$

A = Absorbance at respective wavelength

W = Fresh weight of the sample

V = Volume of extract (mL)

#### **3.5.5 Determination of Lipid peroxidation**

MDA was used as an indicator of lipid peroxidation, and was determined according to Sankhalkar and Sharma (2002). Using mortar and pestle fresh 0.5 g of leaf tissue was extracted in 5 mL of 1% TCA solution. The entire volume was made to 5 mL and centrifuged at 1000 rpm for five minutes to remove the cell debris. To 1 mL of the supernatant 2.5 mL of incubation buffer (150 mM NaCl and 50 mM Tris HCl) and 2.5 mL of 0.5% TBA in 20% TCA were added. The reaction mixture was incubated at 95°C for 30 minutes followed by cooling at room temperature. The absorbance was measured with a UV-Vis spectrophotometer at 600 and 532 nm. Absorbance at 600 nm was subtracted from



absorbance at 532 nm in order to correct for the non-specific turbidity using extinction coefficient of  $155 \text{ mM}^{-1} \text{ cm}^{-1}$ . The MDA concentration is given as  $\text{nmol g}^{-1}$  f.w. of tissue.

### 3.5.6 Proline estimation

Proline was determined by Bates *et al.*, (1973) and it is an indication of osmotic stress. It is produced by interacting with Ninhydrin reagent in an acidic environment to create a chromophore, which was then extracted with toluene and measured spectrophotometrically at 520 nm. Using mortar and pestle, fresh 0.2 g of leaf tissue was weighed and homogenized with 3% Sulfosalicylic acid. The volume was made to 5 mL and was centrifuged at 2500 rpm for 5 minutes. 1 mL of supernatant was treated with 1 mL acid Ninhydrin (1.25 g Ninhydrin, 30 mL GAA, and 20 mL 6M Phosphoric acid) and 1mL of glacial acetic acid. The mixture was incubated at  $95^{\circ}\text{C}$  for 1 h and cooled to room temperature. To this 4 mL of toluene was added and mixed vigorously by shaking. The mixture was allowed to settle to separate the two phases and absorbance of the upper aqueous layer was taken at 520 nm using UV-Visible spectrophotometer. L-Proline was used as a standard for quantification by plotting a standard graph against concentration.

## **CHAPTER 4: RESULTS**

### **4.1 Description of *Getonia floribunda***

The plant sample were collected from Goa University campus. **Plate 4.1A** shows the habit of the plant. It is a climbing shrub which grows to a height of 5-10 m. The vine-covered branches are known to store plenty of water. Keratinous leaves are 5-12 cm long, ovoid or oval in shape, opposite, acuminate, and spherical as seen in **Plate 4.1B**. The dense flower cluster appears at the tips of branches (Yarazari & Jayaraj, 2022). Flowers are devoid of petals as depicted in **Plate 4.1C**. Fruit is fluffy sham-winged about 8 mm long as depicted in **Plate 4.1D**.

### **4.2 Biosynthesis of Iron oxide Nanoparticles**

The green synthesis of iron oxide nanoparticles was initiated by combining 0.1M ferric chloride with the *Getonia floribunda* leaf extract. Upon addition of the leaf extract to  $\text{FeCl}_3$ , an immediate colour shift was observed, indicating rapid nanoparticle formation. The visible transition from yellow to black served as compelling evidence confirming the reduction of Fe ions by the plant extract. This colour change is a physical manifestation of the reduction process, substantiating the successful synthesis of iron oxide nanoparticles. The phytochemicals present in the leaf extract played dual roles as reducing and stabilizing agents, as documented by Bhuiyan *et al.*, (2020). Through their interaction with metal ions, these phytochemicals facilitated the synthesis of iron oxide nanoparticles, ultimately leading to the formation of a black-coloured precipitate.

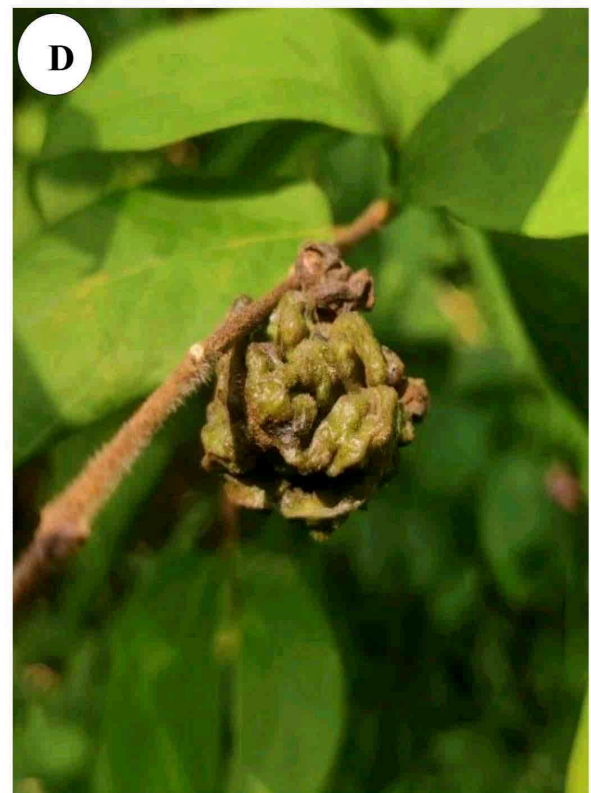
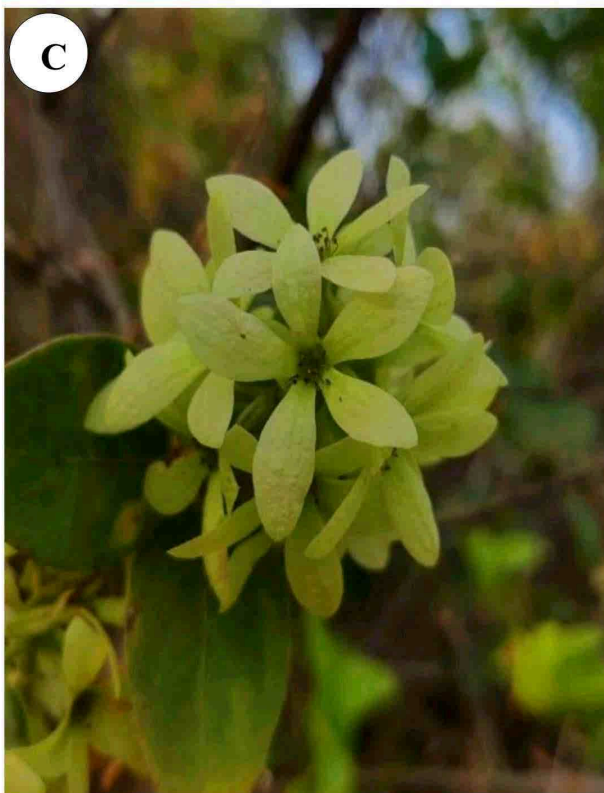


**Plate 4.1:** *Getonia floribunda* A) Habit B) Leaves C) Flowers D) Fruit.

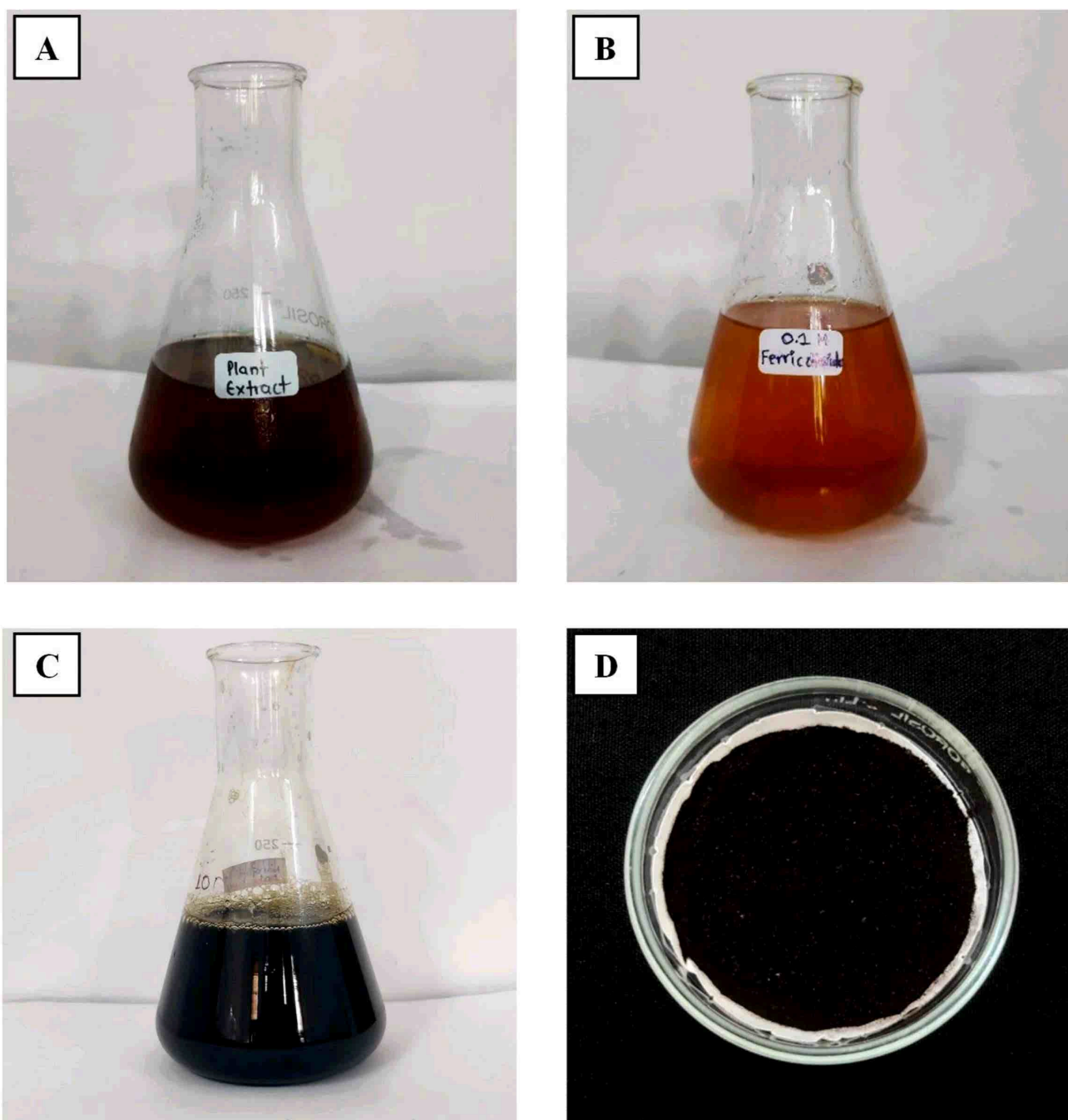


**Plate 4.2:** Green synthesis of iron oxide nanoparticles **A)** Plant extract **B)** Ferric chloride

**C)** Synthesized iron oxide nanoparticles **D)** Dried powder of NPs.

### 4.3 Characterization of Synthesized Iron Oxide Nanoparticles

#### 4.3.1 Analysis of iron oxide nanoparticles using Scanning electron microscopy (SEM) and Energy Dispersive Spectroscopy (EDS)

The morphology of the synthesized iron oxide nanoparticles was examined using Scanning electron microscopy (SEM), as depicted in **Fig. 4.1A**. The nanoparticles exhibited a spherical shape with an average size of 84.6 nm. However, results revealed that the particles were not uniformly distributed and appeared to be agglomerated (**Fig. 4.1B**). This aggregation could be attributed to the presence of different bioactive reducing agents in the plant extract or to the tendency of iron-based nanoparticles to form clusters due to magnetic interactions.

Further characterization via Energy dispersive X-ray spectroscopy (EDS) was conducted to analyse the elemental composition of the nanoparticles. **Fig. 4.1C** illustrates the presence of Fe and O in the sample, along with minor amounts of C and Cl. The weight percentages detected in the irradiated area were 88.34% for Fe and 8.86% for O. The presence of carbon is likely attributed to residual components from the plant extract, while chlorine may be present as impurities formed during the nanoparticle synthesis process.

#### 4.3.2 FTIR analysis of Iron oxide nanoparticles

FTIR analysis was conducted on both the *Getonia floribunda* leaf extract and the synthesized iron oxide nanoparticles to identify the functional groups of phytoconstituents responsible for the reduction of the iron precursor. The analysis was performed over the range of 400-4000  $\text{cm}^{-1}$ .

The FTIR spectrum of the leaf extract (**Fig. 4.2**) exhibited prominent peaks at 3378  $\text{cm}^{-1}$  and 1646  $\text{cm}^{-1}$ , which are characteristic of O-H and C=O functional groups, respectively. Similarly, comparable absorption peaks were observed in the FTIR spectrum of the iron oxide



nanoparticles at  $3381\text{ cm}^{-1}$  and  $1649\text{ cm}^{-1}$ , indicating the presence of these functional groups in the nanoparticles. Additionally, a peak at  $586\text{ cm}^{-1}$  was observed in the nanoparticles' spectrum, which is attributed to the Fe-O bond formation within the sample.

#### 4.3.3 X-ray diffraction (XRD) analysis

The crystalline nature of the biosynthesized iron oxide nanoparticles (IONPs) using *Getonia floribunda* extract was confirmed through X-ray diffraction (XRD) analysis. The XRD pattern of the IONPs is depicted in **Fig. 4.3**, revealed seven distinct peaks at  $2\theta$  values of  $30.300^\circ$ ,  $35.690^\circ$ ,  $43.420^\circ$ ,  $57.290^\circ$ ,  $63.150^\circ$ ,  $71.010^\circ$ , and  $74.350^\circ$ , respectively.

These peaks correspond to the cubic crystalline structure of maghemite ( $\text{Fe}_2\text{O}_3$ ). Furthermore, all these diffraction peaks are in excellent agreement with the standard JCPDS card number 00-025-1402. The intense and sharp nature of the peaks indicates that the  $\text{Fe}_2\text{O}_3$  nanoparticles are crystalline in nature.

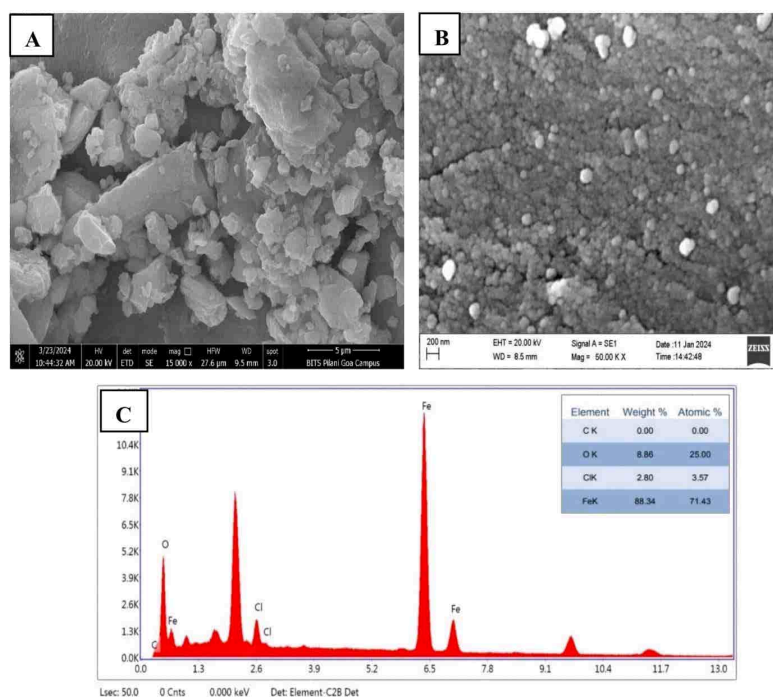


**Figure 4.1:** SEM images of biosynthesized iron oxide nanoparticles at a magnification of 15 000 X (A) and 50.00 KX (B); (C) EDS spectrum of iron oxide NPs.

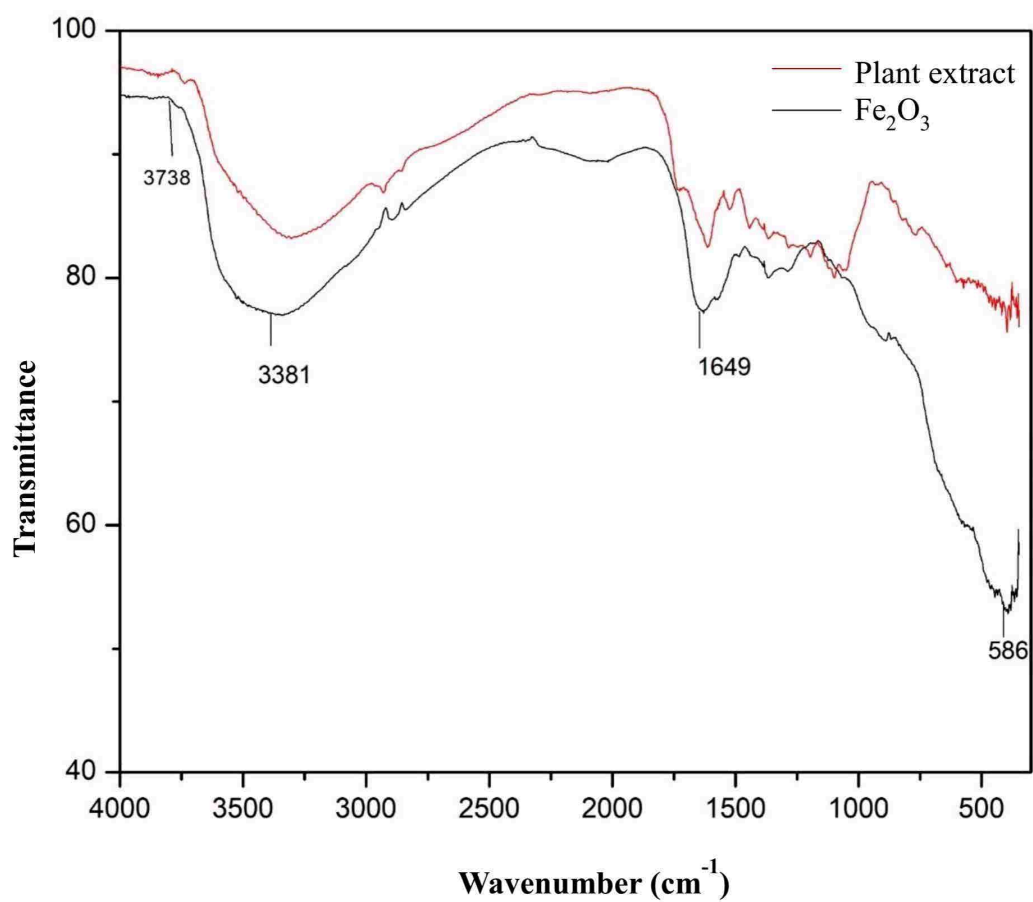


**Figure 4.2.** FTIR spectra of the *Getonia floribunda* leaf extract and synthesized Iron oxide ( $\text{Fe}_2\text{O}_3$ ) nanoparticles.



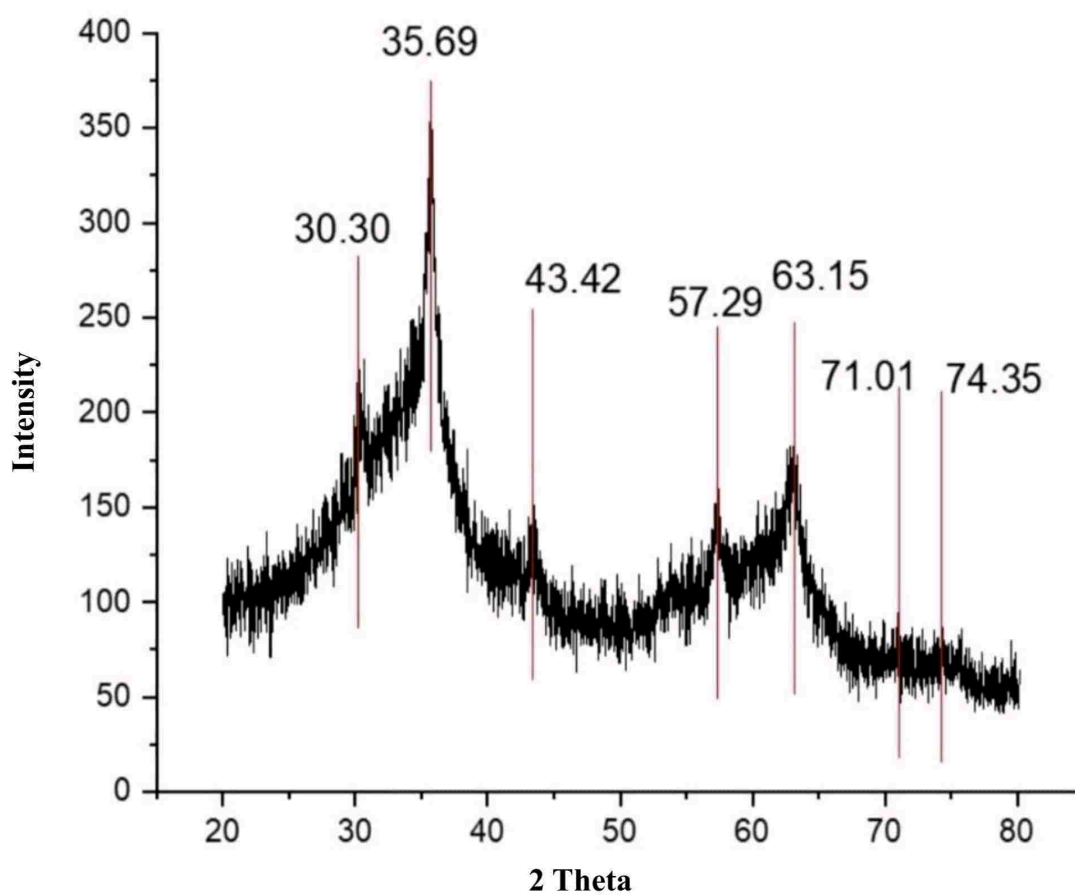


**Figure 4.3.** XRD patterns of iron oxide nanoparticles.

#### 4.4 Degradation study of Rhodamine 6G dye

Photocatalytic degradation of Rhodamine 6G occurred in the presence of iron oxide nanoparticles in a dose-dependent manner. As the dye solution was exposed to sunlight with varying concentrations of nanoparticles, the intense color of the dye gradually faded to colorless in a manner proportional to the nanoparticle concentration. The degradation efficiency increased with increasing nanoparticle concentration, reaching 29.1%, 46.8%, 58.2%, 69.9%, and 72.4% at nanoparticle concentrations of 0.2, 0.4, 0.6, 0.8, and 1.0 g/L, respectively, as illustrated in **Fig. 4.4**.

Moreover, in the absence of catalyst, no degradation of Rhodamine 6G was observed even after 48 hours, regardless of exposure to sunlight or darkness. This underscores the crucial role of the synthesized nanoparticles as catalysts for the degradation of Rhodamine 6G dye. Additionally, an increase in reaction time correlated with enhanced decolorization of the dye, as depicted in **Fig. 4.5** and **Fig. 4.6**. This observation further supports the efficacy of the synthesized nanoparticles as catalysts for the degradation process.

Overall, these findings underscore the potential of the synthesized nanoparticles as efficient and environmentally friendly catalysts for the degradation of Rhodamine 6G dye, highlighting their promising application in wastewater treatment and environmental remediation.

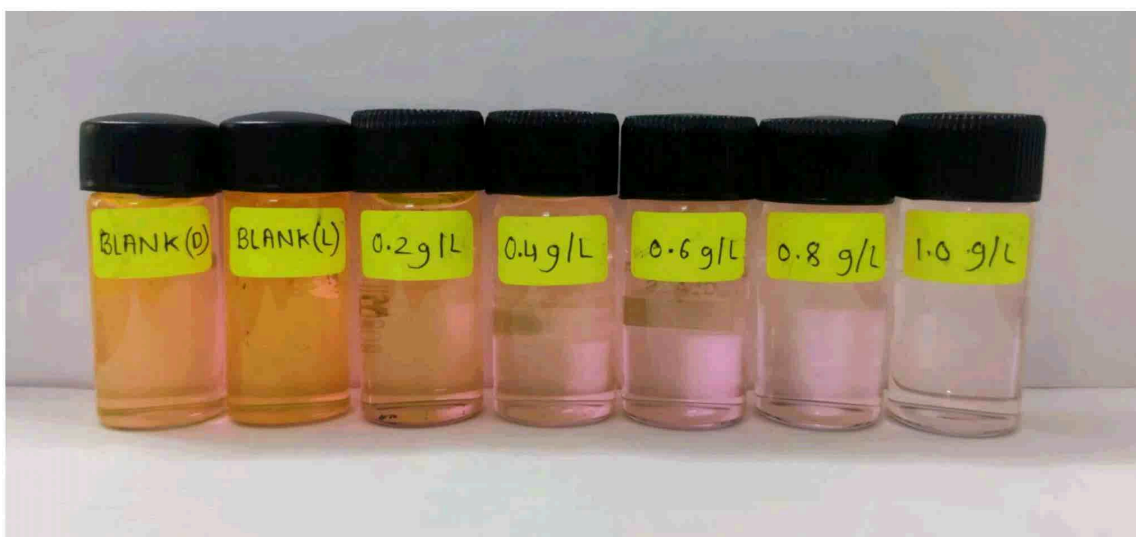


**Plate 4.3:** Photocatalytic degradation of Rhodamine 6G dye treated with different concentration of NPs.

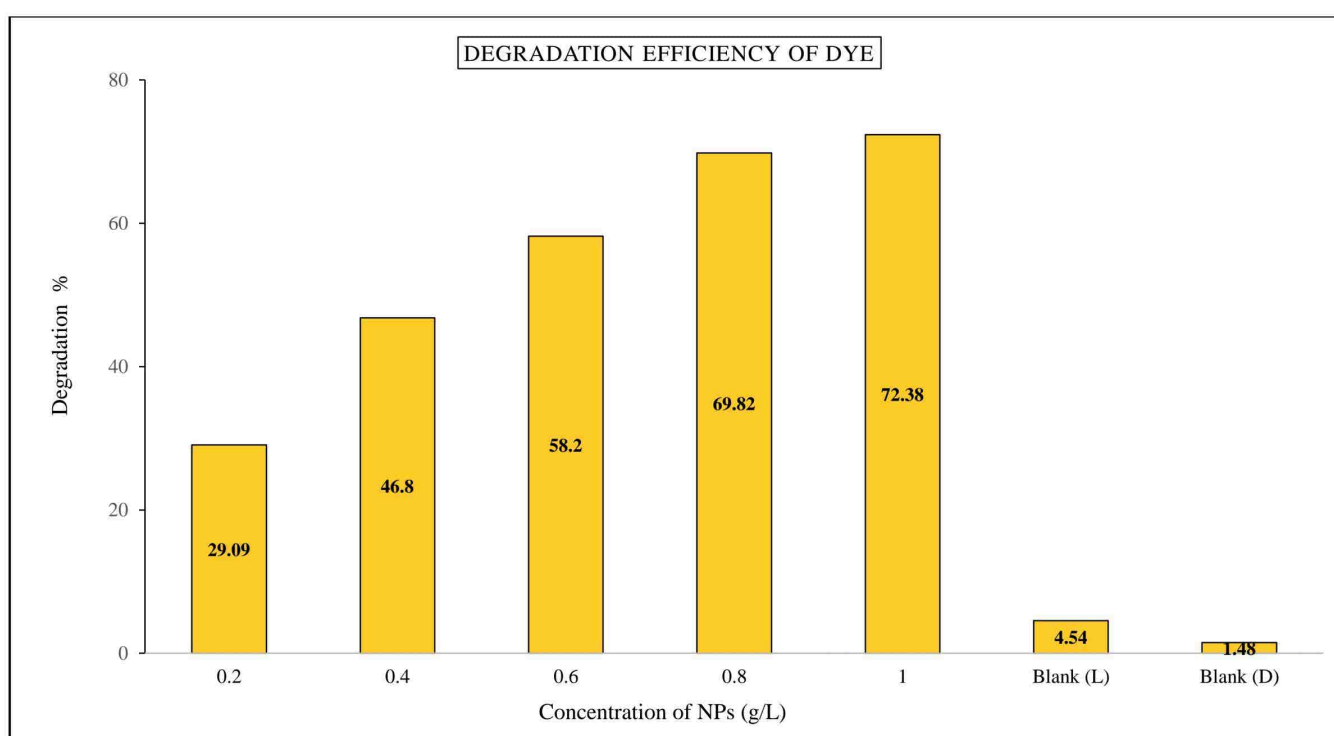


**Figure 4.4.** Graphical representation showing degradation efficiency of Rhodamine 6G dye.

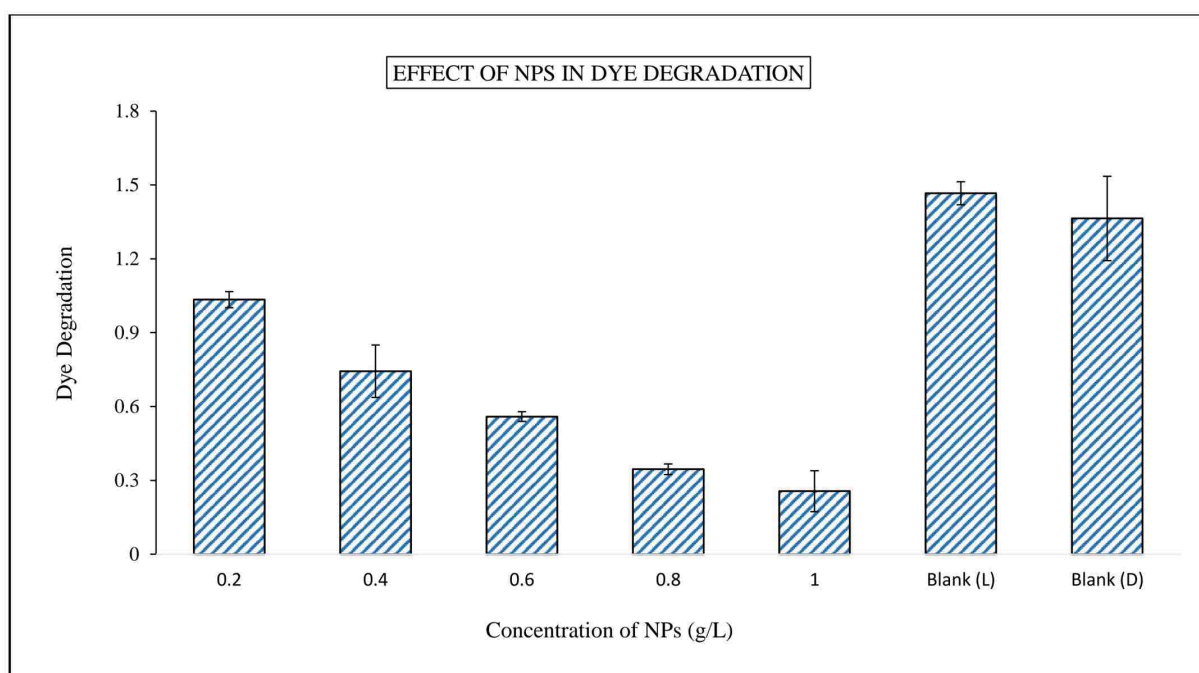


**Figure 4.5.** Effect of different concentration of iron oxide nanoparticles in degradation of Rhodamine 6G dye.

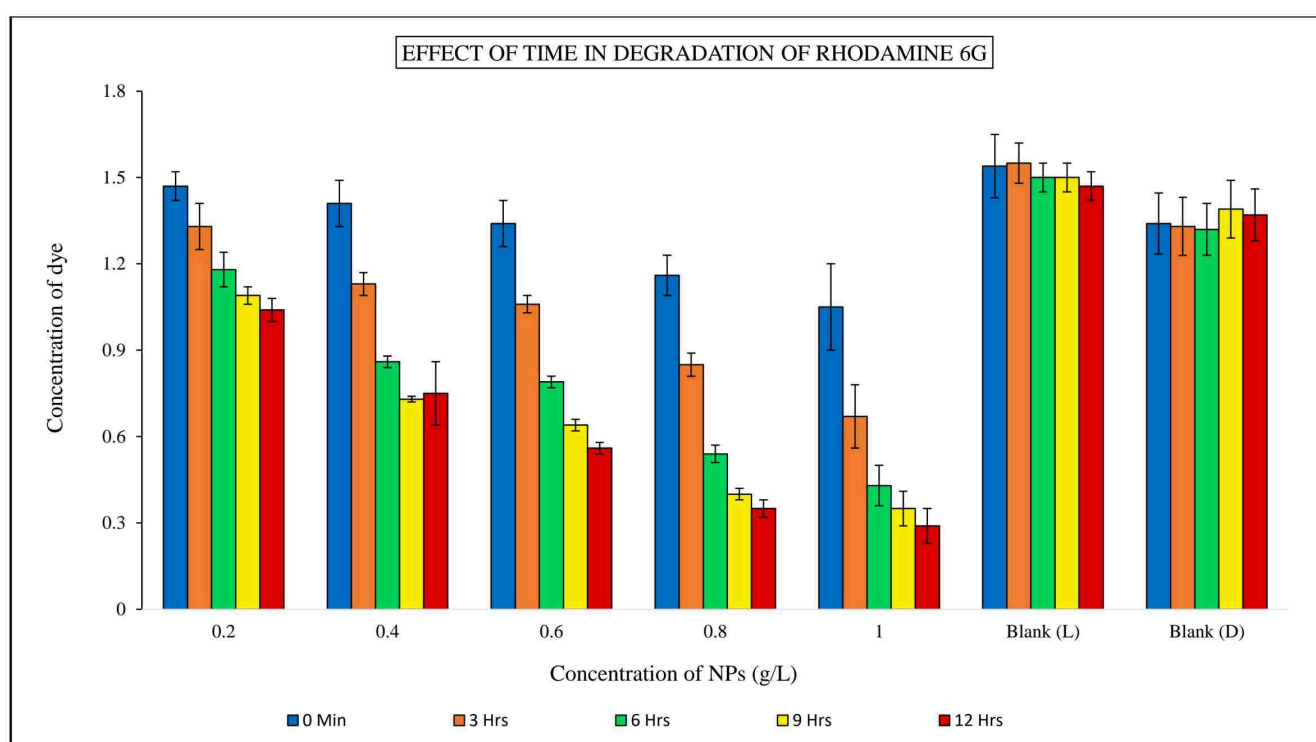


**Figure 4.6.** Effect of time in degradation of Rhodamine 6G with different concentration of NPs.

#### **4.5 Effect of degraded dye on rice seedlings**

The study evaluated the impact of nanoparticle-mediated degradation of Rhodamine 6G (R6G) dye on *Oryza sativa* cv. Jaya seedlings, focusing on parameters such as plant growth, biomass, chlorophyll content, and stress indicators including Malondialdehyde (MDA) and Proline accumulation.

The findings revealed significant effects on plant growth and physiological parameters. Seedlings exposed to nanoparticle-mediated degraded dye exhibited alterations in growth patterns and biomass accumulation compared to the control group. Notably, changes in chlorophyll content were observed, indicative of potential stress responses induced by the degraded dye. Furthermore, the assessment of stress indicators, including Malondialdehyde (MDA) and Proline accumulation, highlighted elevated levels in seedlings exposed to the dye. This suggests oxidative damage and physiological stress responses in the plants subjected to the degraded dye. Overall, these findings underscore the importance of understanding the effects of degraded dye on rice seedlings and the necessity for further research to elucidate the underlying mechanisms. Additionally, there is a pressing need to develop strategies to mitigate the impact of environmental pollutants on agricultural ecosystems, emphasizing the significance of Fe<sub>2</sub>O<sub>3</sub> nanoparticle-mediated degradation as a potential solution.

##### **4.5.1 Effect of degraded dye on plant biomass and Shoot/Root length**

The effect of nanoparticle-induced degraded Rhodamine 6G (R6G) dye on plant biomass, shoot, and root length was assessed in this study. Shoot/root length and biomass were calculated for each experimental set, with the percentage increase or decrease compared to the control.

Plants treated with 0.2 and 0.4 g/L concentrations of nanoparticle-mediated degraded dye exhibited a decrease in shoot length by 26.7% and 23.2%, and a decrease in root length by 25.9% and 18.1%, respectively, compared to the control. Similarly, at 0.6, 0.8, and 1.0 g/L concentrations of nanoparticle-mediated R6G dye, the shoot length decreased by 13%, 8.7%, and 4.5%, and root length decreased by 15%, 11.3%, and 3.5%, respectively, compared to the control. Interestingly, it was observed that with increasing concentrations of nanoparticles up to 1 g/L, there was an increased biomass, shoot, and root length compared to the 0.2 g/L concentration of nanoparticle-mediated R6G degradation. This suggests a dose-dependent increase in plant growth parameters with higher nanoparticle concentrations, indicating the potential protective effect of *Getonia*-induced iron oxide nanoparticles on plant growth (**Table 4.1; Fig. 4.7**).

Furthermore, plants treated with 0.2 and 0.4 g/L concentrations of nanoparticles showed a decrease in shoot biomass by 19.7% and 16.1%, and a decrease in root biomass by 38.5% and 33.4%, respectively, compared to the control. Similarly, plants treated with 0.6, 0.8, and 1.0 g/L showed decreases in shoot biomass by 12.4%, 9.9%, and 3.8%, and decreases in root biomass by 28.2%, 25.7%, and 12.9%, respectively, compared to the control. Despite these decreases, the overall trend of increased biomass, shoot, and root length with increasing concentration of *Getonia*-induced iron oxide nanoparticles suggests a beneficial role in promoting plant growth (**Table 4.1; Fig. 4.8**).

While there were decreases in plant biomass and shoot/root length at lower concentrations of nanoparticles, the overall protective effect of nanoparticles on plant growth was evident with increasing concentrations. This highlights the potential of nanoparticles in degrading R6G dye while also providing protection to plants, as evidenced by increased biomass and shoot/root length with higher nanoparticle concentrations.



These findings emphasize the detrimental effects of degraded dye on plant growth and underscore the importance of understanding dose-dependent responses in assessing the impact of environmental pollutants on agricultural ecosystems. Notably, the study revealed that increasing concentrations of  $\text{Fe}_2\text{O}_3$  nanoparticles mediated dye degradation corresponded with an increase in plant biomass, suggesting a potential protective role against the adverse effects of environmental pollutants on plant growth and agricultural ecosystems.



**Plate 4.4:** Photographic image of 15 days old *Oryza sativa* cv. Jaya seedlings treated with different concentration of degraded dye. **A)** Experimental setup; **B)** Root/ shoot length.

**Table 4.1.** Effect of degraded dye on the shoot, root length and biomass (shoot and root) in 15 days old rice seedlings. Data represents mean value  $\pm$  standard deviation (n=3).

<i>Sr. No.</i>	Nanoparticle Treatment	Shoot length (cm)	Root length (cm)	Biomass (grams)	
				Shoot	Root
1.	Control	18.94 $\pm$ 1.37	8.51 $\pm$ 0.44	0.81 $\pm$ 0.01	0.39 $\pm$ 0.02
2.	0.2 g/L	13.9 $\pm$ 0.11	6.31 $\pm$ 0.4	0.65 $\pm$ 0.06	0.24 $\pm$ 0.01
3.	0.4 g/L	14.55 $\pm$ 0.93	6.97 $\pm$ 0.06	0.68 $\pm$ 0.01	0.26 $\pm$ 0.02
4.	0.6 g/L	16.48 $\pm$ 0.47	7.23 $\pm$ 0.17	0.71 $\pm$ 0.08	0.28 $\pm$ 0.04
5.	0.8 g/L	17.3 $\pm$ 0.55	7.55 $\pm$ 0.84	0.73 $\pm$ 0.01	0.29 $\pm$ 0.01
6.	1.0 g/L	18.1 $\pm$ 0.36	8.21 $\pm$ 0.62	0.78 $\pm$ 0.07	0.34 $\pm$ 0.06

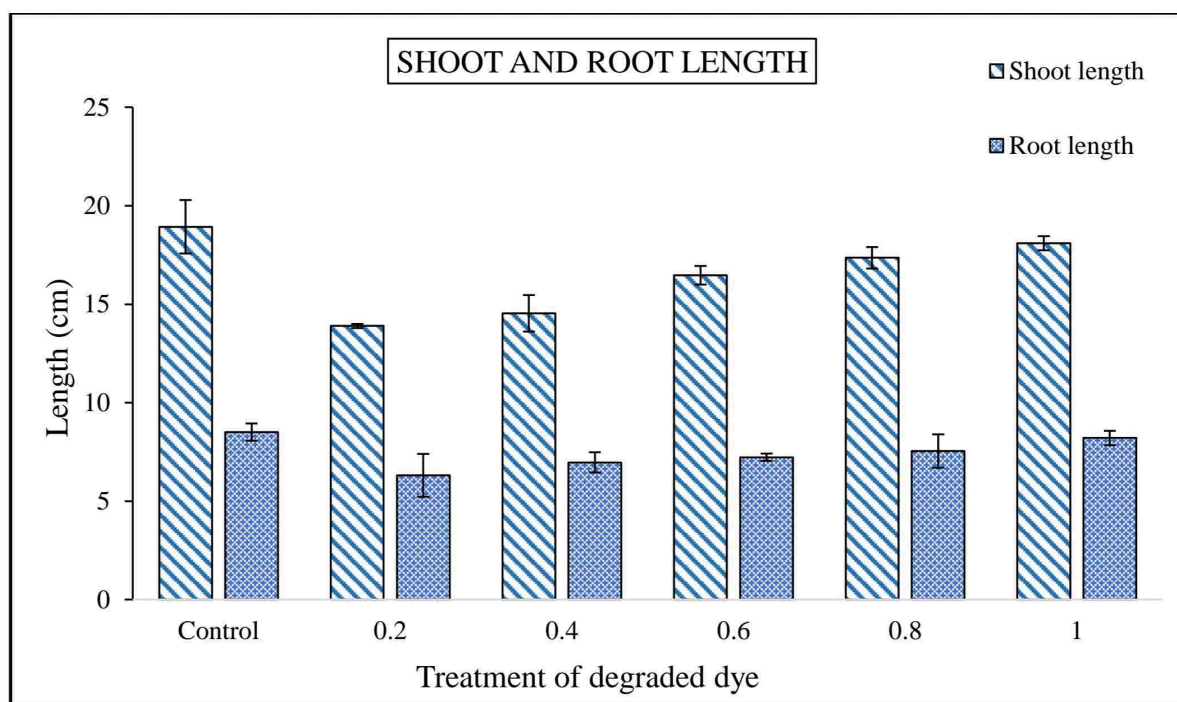


**Figure 4.7.** Effect of degraded dye on the shoot and root length of rice.

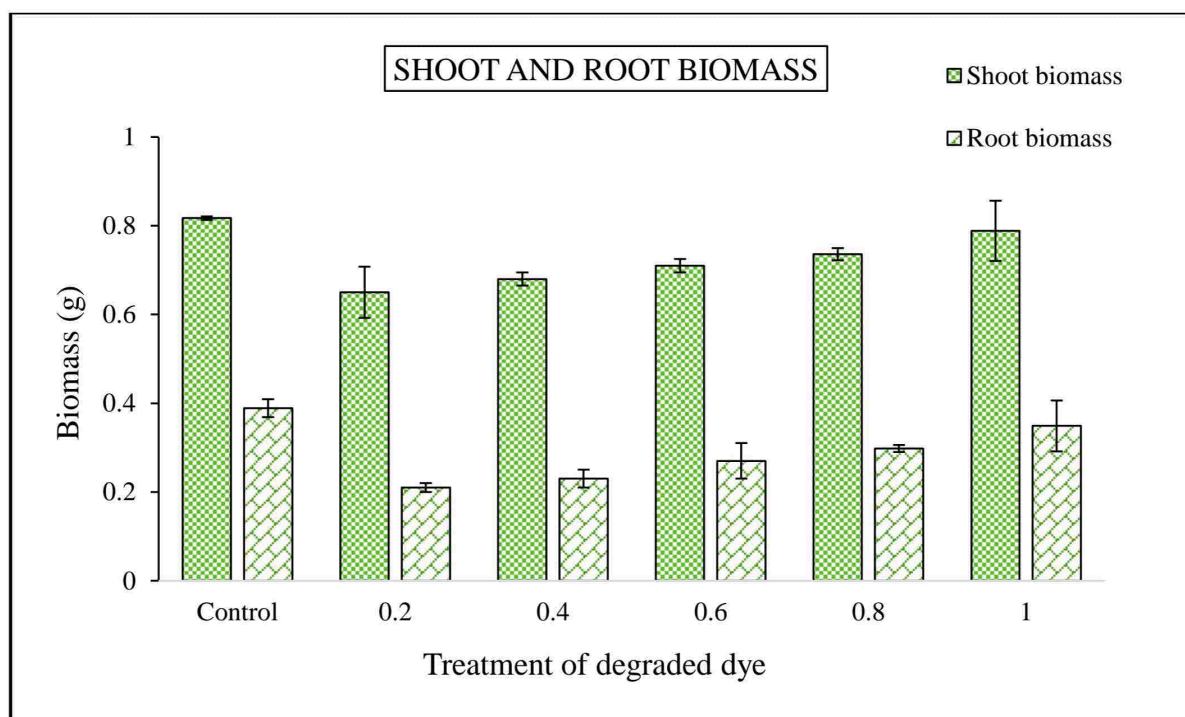


**Figure 4.8.** Effect of degraded dye on the shoot and root biomass of rice.

#### 4.5.2 Estimation of chlorophyll content

Chlorophyll content was estimated in all treated sets, revealing a decrease compared to the control, as depicted in **Table 4.2** and **Fig. 4.9**. Plants treated with 0.2 and 0.4 g/L concentration of nanoparticles against 10 ppm concentration of R6G showed a significant reduction in chlorophyll content, by 77.7% and 69.5%, respectively, compared to control plants. Similarly, treatments with 0.6, 0.8, and 1.0 g/L led to reductions in chlorophyll content by 63.9%, 55.6%, and 16.7%, respectively, relative to the control. Furthermore, a trend was observed where chlorophyll content increased with a decrease in the concentration of degraded dye (**Fig. 4.9**).

Moreover, it is noteworthy to emphasize that with increasing concentrations of nanoparticle-induced R6G dye, the chlorophyll content exhibited an increasing trend. This indicates that the dye was effectively degraded with higher concentrations of *Getonia*-mediated nanoparticles exposed to sunlight. The concurrent increase in chlorophyll content suggests a potential beneficial effect on plant photosynthetic activity.

This observation implies that the degradation of R6G dye by nanoparticles not only mitigated the adverse effects of dye contamination but also promoted chlorophyll synthesis and photosynthetic efficiency in the treated plants. Such findings highlight the dual benefits of Fe<sub>2</sub>O<sub>3</sub> nanoparticle-mediated dye degradation in enhancing plant health and environmental sustainability.

**Table 4.2.** Effect of different concentration of degraded dye on the chlorophyll content of rice seedlings. Data represents mean value  $\pm$  standard deviation (n=3).

Concentration of degraded dye	Chlorophyll content (Mg/g fr.wt.)
Control	0.36 $\pm$ 0.02
0.2 g/L	0.08 $\pm$ 0
0.4 g/L	0.11 $\pm$ 0.03
0.6 g/L	0.13 $\pm$ 0.03
0.8 g/L	0.16 $\pm$ 0.02
1.0 g/L	0.3 $\pm$ 0.02

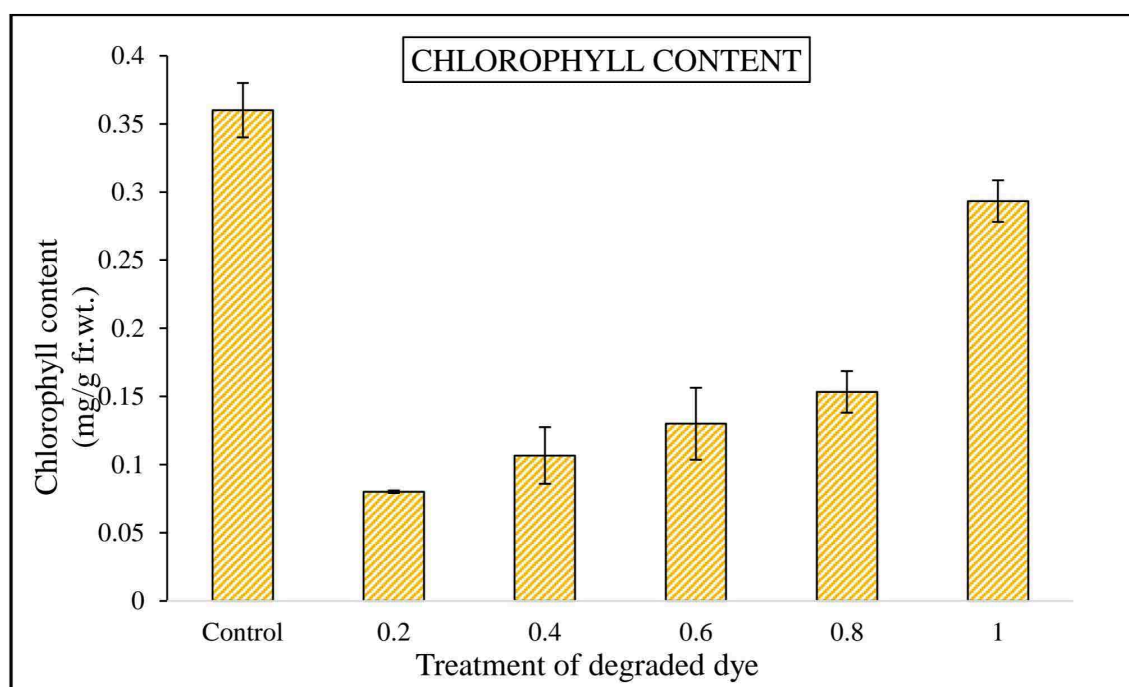


**Figure 4.9.** Effect of different concentration of degraded dye on the Chlorophyll content of Rice seedlings. Vertical bars represent the standard deviation (n=3).



### 4.5.3 Determination of lipid peroxidation

The level of lipid peroxidation, determined by measuring the MDA content, exhibited an increase in treated plants compared to the control. Plants treated with 0.2 and 0.4 g/L showed a notable increase in MDA content, with increments of 50% and 33.4%, respectively, compared to the control (**Table 4.3** and **Fig. 4.10**). Additionally, there were observed increases of 27.3%, 20%, and 11.2% in MDA content in plants treated with 0.6, 0.8, and 1.0 g/L respectively, relative to the control (**Fig. 4.10**). This trend indicates a decrease in MDA content as the concentration of degraded dye decreases.

Moreover, it is noteworthy that with increasing concentrations of *Getonia*-induced nanoparticles (NPs), the level of lipid peroxidation declined from 0.2 g/L to 1 g/L concentration of NP-mediated dye degradation. This suggests a potential protective effect of nanoparticle-induced dye degradation against lipid peroxidation, indicative of reduced oxidative stress in the treated plants.

Such findings underscore the effectiveness of Fe<sub>2</sub>O<sub>3</sub> nanoparticle-mediated dye degradation in mitigating lipid peroxidation and oxidative stress in plants. This highlights the potential of nanoparticle-based remediation strategies in promoting plant health and resilience in the face of environmental pollutants.

**Table 4.3.** Effect of different concentration of degraded dye on Malondialdehyde level of rice seedlings. Data represents mean value  $\pm$  standard deviation (n=3).

Concentration of degraded dye	MDA content ( $\mu\text{mol g}^{-1}$ fr.wt.)
Control	0.6 $\pm$ 0.01
0.2 g/L	0.16 $\pm$ 0.01
0.4 g/L	0.12 $\pm$ 0.01
0.6 g/L	0.11 $\pm$ 0.01
0.8 g/L	0.1 $\pm$ 0.01
1.0 g/L	0.09 $\pm$ 0.01

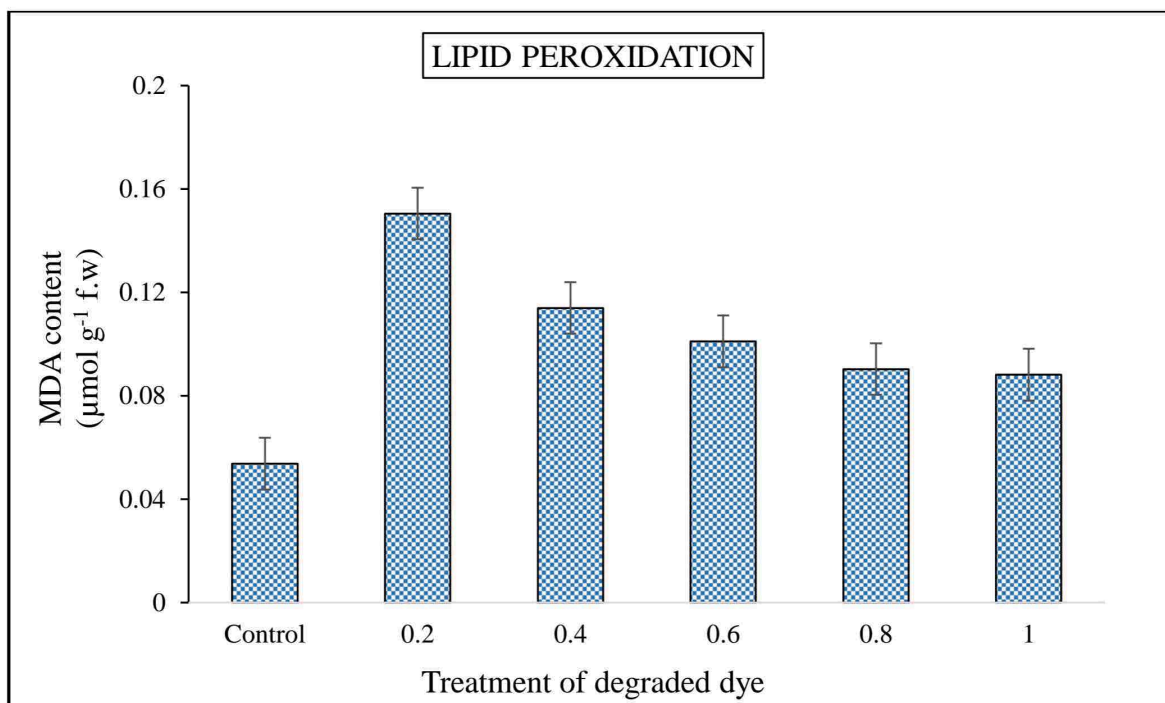


**Figure 4.10.** Effect of different concentration of degraded dye on the lipid peroxidation (MDA) of rice seedlings. Vertical bars represent the standard deviation (n=3).



#### 4.5.4 Effect of degraded dye on proline accumulation

The effect of degraded dye on proline accumulation revealed a notable trend across different concentrations. As illustrated in **Table 4.4** and **Fig. 4.11**, there was a decrease in proline content with a decrease in the concentration of degraded dye.

Initially, plants treated with 0.2 and 0.4 g/L degraded dye showed a significant increase in proline content, with increments of 88.1% and 77.4%, respectively, compared to the control. However, as the concentration of the dye decreased, notably at 0.6, 0.8, and 1.0 g/L, proline content increased by 65.2%, 59.9%, and 54.9%, respectively, relative to the control (**Fig. 4.11**).

This observed trend aligns with previous findings in this study, indicating a consistent pattern of proline accumulation in response to 10 ppm concentration degraded dye mediated by increasing concentrations of *Getonia*-induced Fe<sub>2</sub>O<sub>3</sub> nanoparticles. The decrease in proline content with decreasing concentrations of the coloured dye mediated by increasing concentration of iron oxide nanoparticles suggests a potential regulatory mechanism in response to environmental stressors.

These findings imply that proline accumulation serves as a response mechanism to the presence of degraded dye, with higher concentrations eliciting a greater stress response. The decrease in proline content at higher concentrations of Fe<sub>2</sub>O<sub>3</sub> nanoparticles may indicate a reduction in stress levels, reflecting the adaptive capacity of plants to environmental challenges.

**Table 4.4.** Effect of different concentration of degraded dye on proline in  $\mu\text{molg}^{-1}$  fr.wt. of rice seedlings. Data represents mean value  $\pm$  standard deviation (n=3).

Concentration of degraded dye	Proline ( $\mu\text{molg}^{-1}$ fr.wt.)
Control	0.94 $\pm$ 0.07
0.2 g/L	7.85 $\pm$ 0.85
0.4 g/L	4.15 $\pm$ 0.44
0.6 g/L	2.7 $\pm$ 0.59
0.8 g/L	2.34 $\pm$ 0.32
1.0 g/L	2.08 $\pm$ 0.24

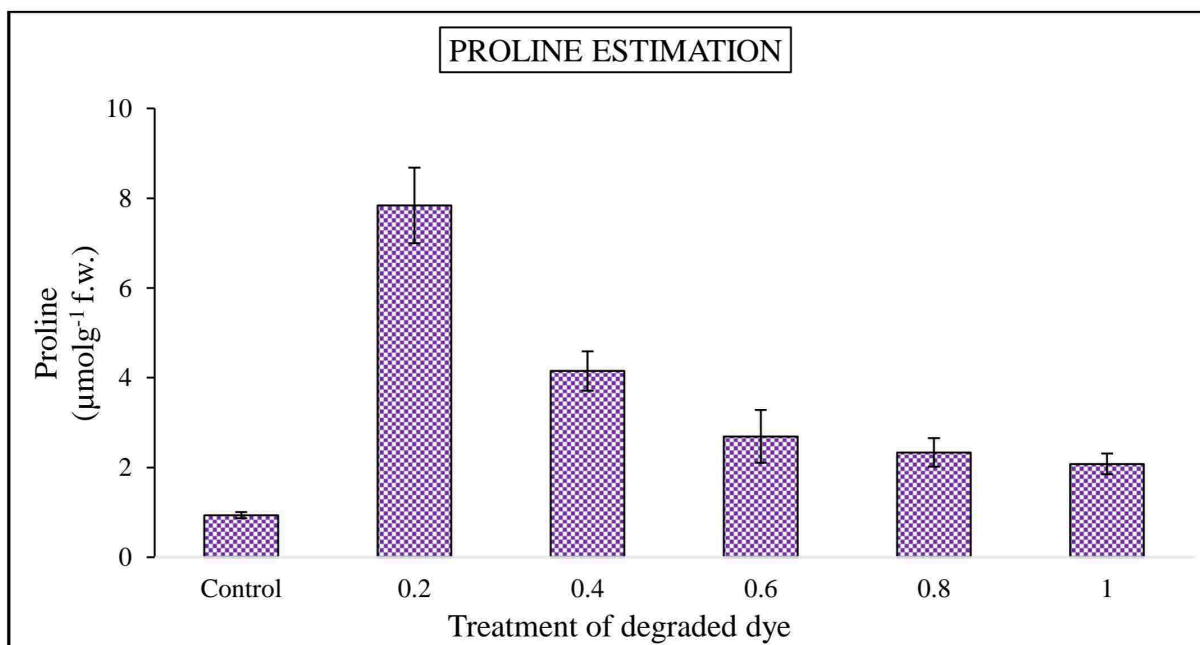


**Figure 4.11.** Accumulation of proline in the leaves of rice seedlings treated with different concentration of degraded dye. Vertical bars represent the standard deviation (n=3).

## **CHAPTER 5: DISCUSSION**

The outcomes of our investigation into the green synthesis of iron oxide nanoparticles (IONPs) using *G. floribunda* exhibit striking parallels with prior research. Upon the addition of leaf extract to  $\text{FeCl}_3$ , an immediate color change signified the rapid formation of NPs, consistent with findings reported by Bhuiyan *et al.*, (2020). The dark coloration of the IONPs is attributed to surface plasmon excitation vibrations, corroborating observations made by Adhikari *et al.*, (2022).

FTIR analysis revealed the presence of various functional groups within the plant extract, serving as both reducing and capping agents during IONP synthesis, aligning with the findings of Adhikari *et al.*, (2022). Specifically, bands at  $3381\text{ cm}^{-1}$  and  $1649\text{ cm}^{-1}$  corresponding to O-H and C=O groups, respectively, were identified in the plant extract. Following IONP synthesis, a new absorption peak emerged at  $586\text{ cm}^{-1}$ , attributed to the Fe-O group, a distinguishing feature of  $\text{Fe}_2\text{O}_3$  spectra, as reported in prior studies (Badmapriya and Asharani, 2016).

These consistent findings underscore the reliability and reproducibility of the green synthesis method employed, highlighting the robustness of *G. floribunda*-mediated nanoparticle fabrication. The presence of characteristic functional groups and spectral signatures further elucidates the mechanistic insights behind the synthesis process, affirming its efficacy and potential for various applications, particularly in environmentally benign nanotechnology.

The SEM images revealed that the IONPs synthesized using *G. floribunda* were spherical and slightly agglomerated. The agglomeration was due to the lower capping ability of plant extract or may be due to magnetic interactions of iron-based NPs (Adhikari *et al.*, 2022). The average particle size of IONPs was found to be 84.6 nm. The presence of

elemental iron and oxygen was confirmed by EDS analysis along with small amount of carbon which was due to the presence of phenolic compounds in the plant extract. The similar results for  $\text{Fe}_2\text{O}_3$  were reported by Bibi *et al.*, (2019) using *Punica granatum* seed extract. Our results from XRD showed that the synthesized NPs were cubic crystalline in nature.

The elemental composition, confirmed through EDS analysis, demonstrated the presence of elemental iron and oxygen, supplemented by a minor amount of carbon derived from the phenolic compounds within the plant extract. This observation echoes findings reported by Bibi *et al.*, (2019) in their investigation utilizing *Punica granatum* seed extract.

Furthermore, XRD analysis corroborated the crystalline nature of the synthesized nanoparticles, showcasing a cubic crystalline structure reminiscent of  $\text{Fe}_2\text{O}_3$ , consistent with previous research. These combined findings affirm the successful synthesis of iron oxide nanoparticles utilizing *G. floribunda*, providing valuable insights into their structural and compositional attributes. Such knowledge enhances their potential for diverse applications across various fields.

Our degradation study revealed the efficacy of iron oxide nanoparticles as photocatalysts for the decolorization of Rhodamine 6G dye, showcasing their excellent activity in dye degradation. Similar findings were reported in the degradation of reactive blue 4 dye (Bibi *et al.*, 2019), further validating the effectiveness of IONPs in pollutant remediation.

Rice, being a staple food rich in carbohydrates, serves as a crucial component of global food security. Our investigation delved into the impact of varying concentrations of degraded dye on rice seedlings. The results indicate that as the concentration of dye increases, there is a corresponding decrease in shoot/root length and biomass. Conversely, a

reduction in dye concentration resulted in an increase in shoot/root length and biomass (Pokharia & Singh, 2015). This growth pattern was hindered in the presence of concentrated dye due to the toxic chemical components inherent in the dye (Surendra *et al.*, 2020).

Our study further unveiled a noteworthy correlation between the concentration of degraded dye and the physiological responses of plants. Specifically, a decrease in dye concentration corresponded to an increase in chlorophyll content, alongside a decrease in proline and malondialdehyde (MDA) content. These findings suggest that as the concentration of dye decreases, plants experience reduced stress levels.

Conversely, higher concentrations of dye induced stress responses in plants, as evidenced by decreased chlorophyll content and elevated proline and MDA levels. This underscores the potential threat posed by dye pollution to plant health and growth.

In light of these results, the application of iron oxide nanoparticles (IONPs) emerges as a promising strategy for mitigating the adverse effects of dye contamination on plant physiology. By efficiently degrading Rhodamine 6G dye, IONPs offer a viable solution to alleviate the stress imposed on plants, thereby safeguarding agricultural ecosystems.

## **CHAPTER 6: CONCLUSION**

In this study, a green synthesis approach utilizing *G. floribunda* leaf extract facilitated the efficient synthesis of iron oxide nanoparticles (IONPs). These nanoparticles were characterized using various techniques including SEM, EDS, FTIR, and XRD, revealing their crystalline nature, spherical shape, and an average size of 84.6 nm. Despite being in agglomerated form, the presence of elemental iron and oxygen was confirmed, affirming the successful synthesis of IONPs.

The synthesized IONPs demonstrated promising photocatalytic activity for the decolorization of Rhodamine 6G dye, with the highest degradation efficiency observed at a concentration of 1.0 g/L. This efficacy increased with higher nanoparticle concentrations, indicating the potential of IONPs as effective catalysts for dye degradation. Furthermore, the study assessed the impact of varying concentrations of degraded dye on *Oryza sativa* seedlings. It was observed that higher concentrations of degraded dye induced stress in the plants, as evidenced by increased proline and malondialdehyde (MDA) content. However, as the concentration of the dye decreased, a corresponding decrease in proline and MDA content was observed, suggesting a reduction in plant stress levels.

These findings underscore the potential of green-synthesized IONPs as catalysts for dye degradation, offering a sustainable solution to mitigate the adverse effects of dye pollution on agricultural ecosystems. Nonetheless, further research is warranted to elucidate the optimal dosage and role of IONPs in alleviating plant stress and promoting sustainable agricultural practices. By continuing to explore the applications of IONPs, we can contribute to the development of eco-friendly strategies for environmental remediation and agricultural sustainability.

## **REFERENCES**

- Abdullah, P. S., Wen, L. K., Awang, H., & Azmin, S. N. H. M. (2021). Rhodamine 6G removal from aqueous solution with coconut shell-derived nanomagnetic adsorbent composite (Cs-nmac): Isotherm and kinetic studies. *Pertanika Journal of Science and Technology*.
- Adhikari, A., Chhetri, K., Acharya, D., Pant, B., & Adhikari, A. (2022). Green synthesis of iron oxide nanoparticles using *Psidium guajava* L. leaves extract for degradation of organic dyes and anti-microbial applications. *Catalysts*, 12(10), 1188.
- Agarwal, H., Kumar, S. V., & Rajeshkumar, S. (2017). A review on green synthesis of zinc oxide nanoparticles—An eco-friendly approach. *Resource-Efficient Technologies*, 3(4), 406-413.
- Aigbe, U. O., Maluleke, R., Lebepe, T. C., Oluwafemi, O. S., & Osibote, O. A. (2023). Rhodamine 6G Dye Adsorption Using Magnetic Nanoparticles Synthesized With the Support of *Vernonia Amygdalina* Leaf Extract (Bitter Leaf). *Journal of Inorganic and Organometallic Polymers and Materials*, 1-20.
- Ait-Touchente, Z., Khalil, A. M., Simsek, S., Boufi, S., Ferreira, L. F. V., Rei Vilar, M., & Chehimi, M. M. (2020). Ultrasonic effect on the photocatalytic degradation of Rhodamine 6G (Rh6G) dye by cotton fabrics loaded with TiO<sub>2</sub>. *Cellulose*, 27, 1085-1097.
- Alexis, F., Rhee, J. W., Richie, J. P., Radovic-Moreno, A. F., Langer, R., & Farokhzad, O. C. (2008, January). New frontiers in nanotechnology for cancer treatment. In *Urologic oncology: seminars and original investigations* (Vol. 26, No. 1, pp. 74-85). Elsevier.

- Ali, A., Zafar, H., Zia, M., ul Haq, I., Phull, A. R., Ali, J. S., & Hussain, A. (2016). Synthesis, characterization, applications, and challenges of iron oxide nanoparticles. *Nanotechnology, science and applications*, 49-67.
- Amrutham, S., Maragoni, V., & Guttena, V. (2020). One-step green synthesis of palladium nanoparticles using neem gum (*Azadirachta Indica*): characterization, reduction of Rhodamine 6G dye and free radical scavenging activity. *Applied Nanoscience*, 10, 4505-4511.
- Arularasu, M. V., Devakumar, J., & Rajendran, T. V. (2018). An innovative approach for green synthesis of iron oxide nanoparticles: Characterization and its photocatalytic activity. *Polyhedron*, 156, 279-290.
- Azhagumeena, c., & Bharathi, p. R. (2020). A review on phytochemistry and pharmacology of *Calycopteris floribunda* roxb. Lam.
- Badmapriya, D., & Asharani, I. V. (2016). Dye degradation studies catalysed by green synthesized iron oxide nanoparticles. *International Journal of ChemTech Research*, 9(6), 409-416.
- Barzan, M., & Hajiesmaeilbaigi, F. (2015). Fluorescence quenching of Rhodamine 6G with different concentrations by laser ablated gold nanoparticles. *Optical and Quantum Electronics*, 47(11), 3467-3476.
- Bates, L. S., Waldren, R. P. A., & Teare, I. D. (1973). Rapid determination of free proline for water-stress studies. *Plant and soil*, 39, 205-207.
- Beheshtkhoo, N., Kouhbanani, M. A. J., Savardashtaki, A., Amani, A. M., & Taghizadeh, S. (2018). Green synthesis of iron oxide nanoparticles by aqueous leaf extract of *Daphne mezereum* as a novel dye removing material. *Applied Physics A*, 124, 1-7.



- Bharat, B. V., & Nagarale, S. (2019). Green synthesis for antimicrobial and anticancer assessments of isolated bioactive compound from *Calycopteris floribunda* leaves. *Journal of Pharmacognosy and Phytochemistry*, 8(3), 4860-4866.
- Bhat, P. R., Prajna, P. S., Kumar, V., Hegde, M. A., & Singh, L. (2011). Antimicrobial properties of leaves of *Calycopteris floribunda* Lam. *Journal of Medicinal Plants Research*, 5(12), 2448-2451.
- Bhuiyan, M. S. H., Miah, M. Y., Paul, S. C., Aka, T. D., Saha, O., Rahaman, M. M., & Ashaduzzaman, M. (2020). Green synthesis of iron oxide nanoparticle using *Carica papaya* leaf extract: application for photocatalytic degradation of remazol yellow RR dye and antibacterial activity. *Heliyon*, 6(8).
- Bibi, I., Nazar, N., Ata, S., Sultan, M., Ali, A., Abbas, A., & Iqbal, M. (2019). Green synthesis of iron oxide nanoparticles using pomegranate seeds extract and photocatalytic activity evaluation for the degradation of textile dye. *Journal of Materials Research and Technology*, 8(6), 6115-6124.
- da Silva, A. M. B., Serrão, N. O., de Gusmão Celestino, G., Takeno, M. L., Antunes, N. T. B., Iglauer, S., & Maia, P. J. S. (2020). Removal of rhodamine 6G from synthetic effluents using *Clitoria fairchildiana* pods as low-cost biosorbent. *Environmental Science and Pollution Research*, 27, 2868-2880.
- DaCosta, M. V. J. (2016). *Morphological, physiological, biochemical and molecular response of rice seedlings to metallo-nanoparticles* (Doctoral dissertation, Goa University).
- Dash, K. K., Deka, P., Bangar, S. P., Chaudhary, V., Trif, M., & Rusu, A. (2022). Applications of inorganic nanoparticles in food packaging: A comprehensive review. *Polymers*, 14(3), 521.

- Devatha, C. P., Thalla, A. K., & Katte, S. Y. (2016). Green synthesis of iron nanoparticles using different leaf extracts for treatment of domestic waste water. *Journal of cleaner production*, 139, 1425-1435.
- Dey, S. K., Shoeb, M., Rob, T., Nahar, N., Mosihuzzaman, M., & Sultana, N. (2005). Biological and Chemical Studies on *Calycopteris floribunda* leaves. *Dhaka University Journal of Pharmaceutical Sciences*, 4(2), 103-106.
- Ealia, S. A. M., & Saravanakumar, M. P. (2017, November). A review on the classification, characterisation, synthesis of nanoparticles and their application. In *IOP conference series: materials science and engineering* (Vol. 263, No. 3, p. 032019). IOP Publishing.
- Glory, A., Judin, J., Vasudevan, R., & Sumathi, P. (2016). Preliminary phytochemical content and antibacterial activity of Ukshi (*Calycopteris floribunda* Lam.) leaves. *J. Med. Plants Stud*, 4(2), 57-59.
- Gour, A., & Jain, N. K. (2019). Advances in green synthesis of nanoparticles. *Artificial cells, nanomedicine, and biotechnology*, 47(1), 844-851.
- Goutam, S. P., Saxena, G., Roy, D., Yadav, A. K., & Bharagava, R. N. (2020). Green synthesis of nanoparticles and their applications in water and wastewater treatment. *Bioremediation of Industrial Waste for Environmental Safety: Volume I: Industrial Waste and Its Management*, 349-379.
- Hasan, S. (2015). A review on nanoparticles: their synthesis and types. *Res. J. Recent Sci*, 2277, 2502.
- Jacinto, M. J., Silva, V. C., Valladão, D. M. S., & Souto, R. S. (2021). Biosynthesis of magnetic iron oxide nanoparticles: a review. *Biotechnology Letters*, 43, 1-12.

- Joseph Kirubakaran, C., Fang, Z., Sha, C., & Yong, Y. C. (2020). Green synthesis of Ag and Pd nanoparticles for water pollutants treatment. *Water Science and Technology*, 82(11), 2344-2352.
- Kansal, S. K., Singh, M., & Sud, D. (2007). Studies on photodegradation of two commercial dyes in aqueous phase using different photocatalysts. *Journal of hazardous materials*, 141(3), 581-590.
- Karpagavinayagam, P., & Vedhi, C. (2019). Green synthesis of iron oxide nanoparticles using *Avicennia marina* flower extract. *Vacuum*, 160, 286-292.
- Kevat, N. (2018). *Copper Mediated Effect on Photosynthesis, Reactive Oxygen Species Metabolism and Related Molecular Responses in Rice Seedlings* (Doctoral dissertation, Goa University).
- Khayati, G. R., Ghasabe, H. M., Karfarma, M., Khayati, G. R., Ghasabe, H. M., & Karfarma, M. (2015). A survey on the application of oxide nanoparticles for improving concrete processing. *Adv. Concr. Constr.*, 3(2), 145-159.
- Laurent, S., Bridot, J. L., Elst, L. V., & Muller, R. N. (2010). Magnetic iron oxide nanoparticles for biomedical applications. *Future medicinal chemistry*, 2(3), 427-449.
- Pandit, C., Roy, A., Ghotekar, S., Khusro, A., Islam, M. N., Emran, T. B., & Bradley, D. A. (2022). Biological agents for synthesis of nanoparticles and their applications. *Journal of King Saud University-Science*, 34(3), 101869.
- Papadaki, D., Kiriakidis, G., & Tsoutsos, T. (2018). Applications of nanotechnology in construction industry. In *Fundamentals of nanoparticles* (pp. 343-370). Elsevier.

- Parveen, S., Wani, A. H., Shah, M. A., Devi, H. S., Bhat, M. Y., & Koka, J. A. (2018). Preparation, characterization and antifungal activity of iron oxide nanoparticles. *Microbial pathogenesis*, 115, 287-292.
- Pavithra, G. M., Naik, A. S., Siddiqua, S., Vinayaka, K. S., Kekuda, P. T. R., & Mukunda, S. (2013). Antioxidant and antibacterial activity of flowers of *Calycopteris floribunda* (Roxb.) Poiret, *Humboldtia brunonis* Wall and *Kydia calycina* Roxb. *International Journal of Drug Development and Research*, 5(2), 301-310.
- Phoemphoonthanyakit, S., Seeharaj, P., Damrongsak, P., & Locharoenrat, K. (2019). Effect of adsorption characteristics of rhodamine 6G dye solution in Fe<sub>3</sub>O<sub>4</sub> magnetic nanoparticles on fluorescence quantum yield. *Journal of Spectroscopy*, 2019.
- Pokharia, A., & Ahluwalia, S. S. (2015). Toxicological effect of textile dyes and their metabolites: a review. *Current Trends in Biotechnology and Chemical Research/ January-June*, 5(1), 11-17.
- Priya, Naveen, Kaur, K., & Sidhu, A. K. (2021). Green synthesis: An eco-friendly route for the synthesis of iron oxide nanoparticles. *Frontiers in Nanotechnology*, 3, 655062.
- Rasheed, T., Bilal, M., Iqbal, H. M., Hu, H., & Zhang, X. (2017). Reaction mechanism and degradation pathway of rhodamine 6G by photocatalytic treatment. *Water, Air, & Soil Pollution*, 228, 1-10.
- Roy, A., Elzaki, A., Tirth, V., Kajoak, S., Osman, H., Algahtani, A., & Bilal, M. (2021). Biological synthesis of nanocatalysts and their applications. *Catalysts*, 11(12), 1494.
- Salem, S. S., & Fouda, A. (2021). Green synthesis of metallic nanoparticles and their prospective biotechnological applications: an overview. *Biological trace element research*, 199(1), 344-370.

- Sankhalkar, S., & Sharma, P. K. (2002). Protection against photooxidative damage provided by enzymatic and non-enzymatic antioxidant system in sorghum seedlings.
- Sharma, P., Kumari, S., Ghosh, D., Yadav, V., Vij, A., Rawat, P., & Majumder, S. (2021). Capping agent-induced variation of physicochemical and biological properties of  $\alpha$ -Fe<sub>2</sub>O<sub>3</sub> nanoparticles. *Materials Chemistry and Physics*, 258, 123899.
- Sidhu, A. K., Verma, N., & Kaushal, P. (2022). Role of biogenic capping agents in the synthesis of metallic nanoparticles and evaluation of their therapeutic potential. *Frontiers in Nanotechnology*, 3, 801620.
- Singh, J., Dutta, T., Kim, K. H., Rawat, M., Samddar, P., & Kumar, P. (2018). 'Green' synthesis of metals and their oxide nanoparticles: applications for environmental remediation. *Journal of nanobiotechnology*, 16(1), 1-24.
- Siva, G. V., & Benita, L. F. J. (2016). Synthesis, characterization of iron oxide nanoparticles and their applications as nano-fertilizers on some quality characters of ginger (*Zingiber officinale* Rosc.). *Int. J. Sci. Res. Sci. Technol.*, 2, 11-18.
- Subhan, M. A., Choudhury, K. P., & Neogi, N. (2021). Advances with molecular nanomaterials in industrial manufacturing applications. *Nanomanufacturing*, 1(2), 75-97.
- Suppiah, D. D., Julkapli, N. M., Sagadevan, S., & Johan, M. R. (2023). Eco-friendly green synthesis approach and evaluation of environmental and biological applications of Iron oxide nanoparticles. *Inorganic Chemistry Communications*, 152, 110700.
- Surendra, B. S., Shekhar, T. S., Veerabhadraswamy, M., Nagaswarupa, H. P., Prashantha, S. C., Geethanjali, G. C., & Likitha, C. (2020). Probe sonication synthesis of ZnFe<sub>2</sub>O<sub>4</sub>

NPs for the photocatalytic degradation of dyes and effect of treated wastewater on growth of plants. *Chemical Physics Letters*, 745, 137286.

Tiwari, J. N., Tiwari, R. N., & Kim, K. S. (2012). Zero-dimensional, one-dimensional, two-dimensional and three-dimensional nanostructured materials for advanced electrochemical energy devices. *Progress in Materials Science*, 57(4), 724-803.

Vasantharaj, S., Sathiyavimal, S., Senthilkumar, P., LewisOscar, F., & Pugazhendhi, A. (2019). Biosynthesis of iron oxide nanoparticles using leaf extract of *Ruellia tuberosa*: antimicrobial properties and their applications in photocatalytic degradation. *Journal of Photochemistry and Photobiology B: Biology*, 192, 74-82.

VG, V. K., & Prem, A. A. (2018). Green Synthesis and Characterization of Iron Oxide Nanoparticles Using *Phyllanthus Niruri* Extract. *Oriental Journal of Chemistry*, 34(5).

Yaqoob, A. A., Ahmad, H., Parveen, T., Ahmad, A., Oves, M., Ismail, I. M., & Mohamad Ibrahim, M. N. (2020). Recent advances in metal decorated nanomaterials and their various biological applications: a review. *Frontiers in chemistry*, 8, 341.

Yarazari, S. B., & Jayaraj, M. (2022). GC–MS analysis of bioactive compounds of flower extracts of *Calycopteris floribunda* Lam.: A multi potent medicinal plant. *Applied Biochemistry and Biotechnology*, 194(11), 5083-5099.